Article

A Charge-Transfer-Induced Spin Transition in a Discrete Complex: The Role of Extrinsic Factors in Stabilizing Three Electronic Isomeric Forms of a Cyanide-Bridged Co/Fe Cluster

Curtis P. Berlinguette, Alina Dragulescu-Andrasi, Andreas Sieber, Hans-Ulrich Gdel, Catalina Achim, and Kim R. Dunbar

J. Am. Chem. Soc., **2005**, 127 (18), 6766-6779• DOI: 10.1021/ja043162u • Publication Date (Web): 19 April 2005

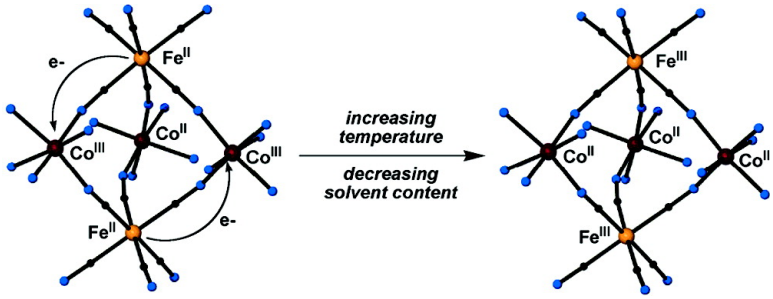

More About This Article

Additional resources and features associated with this article are available within the HTML version:

- Supporting Information
- Links to the 4 articles that cite this article, as of the time of this article download
- Access to high resolution figures
- Links to articles and content related to this article
- Copyright permission to reproduce figures and/or text from this article

View the Full Text HTML

J|A|C|S
ARTICLES
Published on Web 04/19/2005

A Charge-Transfer-Induced Spin Transition in a Discrete Complex: The Role of Extrinsic Factors in Stabilizing Three Electronic Isomeric Forms of a Cyanide-Bridged Co/Fe Cluster

Curtis P. Berlinguette,[†] Alina Dragulescu-Andrasi,[‡] Andreas Sieber,[§] Hans-Ulrich Güdel,[§] Catalina Achim,*[,‡] and Kim R. Dunbar*[,†]

Contribution from the Department of Chemistry, Texas A&M University, P.O. Box 30012, College Station, Texas 77842-3012, Department of Chemistry, Carnegie Mellon University, 4400 Fifth Avenue, Pittsburgh, Pennsylvania 15213, and Department of Chemistry and Biochemistry, University of Bern, Freiestrasse 3, 3000 Bern 9, Switzerland

Received November 12, 2004; E-mail: dunbar@chem.mail.tamu.edu; achim@cmu.edu

Abstract: A series of bimetallic, trigonal bipyramidal clusters of type $\{[Co(N-N)_2]_3[Fe(CN)_6]_2\}$ are reported. The reaction of $\{Co(tmphen)_2\}^{2+}$ with $[Fe(CN)_6]^{3-}$ in MeCN affords $\{[Co(tmphen)_2]_3[Fe(CN)_6]_2\}$ (**1**). The cluster can exist in three different solid-state phases: a red crystalline phase, a blue solid phase obtained by exposure of the red crystals to moisture, and a red solid phase obtained by desolvation of the blue solid phase in vacuo. The properties of cluster **1** are extremely sensitive to both temperature and solvent content in each of these phases. Variable-temperature X-ray crystallography; ^{57}Fe Mössbauer, vibrational, and optical spectroscopies; and magnetochemical studies were used to study the three phases of **1** and related compounds, $Na\{[Co(tmphen)_2]_3[Fe(CN)_6]_2\}(ClO_4)_2$ (**2**), $\{[Co(bpy)_2]_3[Fe(CN)_6]_2\}[Fe(CN)_6]_{1/3}$ (**3**), and $\{[Ni(tmphen)_2]_3[Fe(CN)_6]_2\}$ (**4**). The combined structural and spectroscopic investigation of **1**−**4** leads to the unambiguous conclusion that **1** can exist in different electronic isomeric forms, $\{Co^{III}_2Co^{II}Fe^{II}_2\}$ (**1A**), $\{Co^{III}Co^{II}_2Fe^{III}Fe^{II}\}$ (**1B**), and $\{Co^{II}_3Fe^{III}_2\}$ (**1C**), and that it can undergo a charge-transfer-induced spin transition (CTIST). This is the first time that such a phenomenon has been observed for a Co/Fe molecule.

Introduction

The design of solid-state materials based on molecular precursors has inspired a renaissance in the area of transition metal-cyanide chemistry.[1] This interest has been fueled, in large part, by the quest for new materials with electronic,[2] magnetic,[3,4] and catalytic[5] applications. Indeed, novel magnetic materials inspired by the face-centered 3-D "Prussian-blue" phases have produced high T_c,[6,7] high coercivity,[8−10] porous,[11] and photosensitive[12,13] magnetic materials.

Apart from the recent success in preparing new metal-cyanide solids, low-dimensionality cyanide arrays and clusters have also received a great deal of attention.[14−19] The synthetic strategy typically used to avoid the formation of 3-D phases is the reaction of a cyanometalate anion with a coordinatively unsaturated, convergent metal cationic complex. This approach has successfully produced numerous high-nuclearity clusters, including some with unusually high ground-state spin values.[20−25] The

[†] Texas A&M University.
[‡] Carnegie Mellon University.
[§] University of Bern.

(1) Dunbar, K. R.; Heintz, R. A. *Prog. Inorg. Chem.* **1997**, *45*, 283−391.
(2) Gu, Z. Z.; Sato, O.; Iyoda, T.; Hashimoto, K.; Fujishima, A. *Chem. Mater.* **1997**, *9*, 1092−1097.
(3) Miller, J. S.; Epstein, A. J. *MRS Bull.* **2000**, *25*, 21−28.
(4) Miller, J. S. *MRS Bull.* **2000**, *25*, 60−64.
(5) Yet, L. *Angew. Chem., Int. Ed.* **2001**, *40*, 875−877.
(6) Dujardin, E.; Ferlay, S.; Phan, X.; Desplanches, C.; Moulin, C. C. D.; Sainctavit, P.; Baudelet, F.; Dartyge, E.; Veillet, P.; Verdaguer, M. *J. Am. Chem. Soc.* **1998**, *120*, 11347−11352.
(7) Entley, W. R.; Girolami, G. S. *Science* **1995**, *268*, 397−400.
(8) Kurmoo, M.; Kepert, C. J. *New J. Chem.* **1998**, *22*, 1515−1524.
(9) Manson, J. L.; Kmety, C. R.; Huang, Q. z.; Lynn, J. W.; Bendele, G. M.; Pagola, S.; Stephens, P. W.; Liable-Sands, L. M.; Rheingold, A. L.; Epstein, A. J.; Miller, J. S. *Chem. Mater.* **1998**, *10*, 2552−2560.
(10) Batten, S. R.; Jensen, P.; Moubaraki, B.; Murray, K. S.; Robson, R. *Chem. Commun.* **1998**, 439−440.
(11) Beauvais, L. G.; Long, J. R. *J. Am. Chem. Soc.* **2002**, *124*, 12096−12097.
(12) Dei, A. *Angew. Chem., Int. Ed.* **2005**, *44*, 1160−3.
(13) Sato, O.; Iyoda, T.; Fujishima, A.; Hashimoto, K. *Science* **1996**, *272*, 704−705.
(14) Ohba, M.; Okawa, H.; Fukita, N.; Hashimoto, Y. *J. Am. Chem. Soc.* **1997**, *119*, 1011−1019.
(15) Smith, J. A.; Galan-Mascaros, J. R.; Clerac, R.; Dunbar, K. R. *Chem. Commun.* **2000**, 1077−1078.
(16) Beltran, L. M. C.; Long, J. R. *Acc. Chem. Res.* **2005**, published online February 9, http://dx.doi.org/10.1021/ar040158e.
(17) Oshio, H.; Tamada, O.; Onodera, H.; Ito, T.; Ikoma, T.; Tero-Kubota, S. *Inorg. Chem.* **1999**, *38*, 5686−5689.
(18) Contakes, S. M.; Rauchfuss, T. B. *Angew. Chem., Int. Ed.* **2000**, *39*, 1984−1986.
(19) Klausmeyer, K. K.; Wilson, S. R.; Rauchfuss, T. B. *J. Am. Chem. Soc.* **1999**, *121*, 2705−2711.
(20) Ferbinteanu, M.; Miyasaka, H.; Wernsdorfer, W.; Nakata, K.; Sugiura, K.; Yamashita, M.; Coulon, C.; Clerac, R. *J. Am. Chem. Soc.* **2005**, *127*, 3090−3099.
(21) Wang, S.; Zuo, J.-L.; Zhou, H.-C.; Choi, H. J.; Ke, Y.; Long, J. R.; You, X.-Z. *Angew. Chem., Int. Ed.* **2004**, *43*, 5940−5943.
(22) Larionova, J.; Gross, M.; Pilkington, M.; Andres, H.; Stoeckli-Evans, H.; Gudel, H. U.; Decurtins, S. *Angew. Chem., Int. Ed.* **2000**, *39*, 1605−1609.
(23) Zhong, Z. J.; Seino, H.; Mizobe, Y.; Hidai, M.; Fujishima, A.; Ohkoshi, S.; Hashimoto, K. *J. Am. Chem. Soc.* **2000**, *122*, 2952−2953.
(24) Sokol, J. J.; Hee, A. G.; Long, J. R. *J. Am. Chem. Soc.* **2002**, *124*, 7656−7657.
(25) Berlinguette, C. P.; Vaughn, D.; Canada-Vilalta, C.; Galan-Mascaros, J. R.; Dunbar, K. R. *Angew. Chem., Int. Ed.* **2003**, *42*, 1523−1526.

10.1021/ja043162u CCC: $30.25

primary motivation of these efforts is to obtain paramagnetic molecules that behave as "single-molecule magnets"; i.e., molecules capable of being thermally blocked in a magnetized state.[26−29]

Despite the myriad of known cyanide-bridged discrete clusters, there are limited examples that involve CN^- ligands spanning Co and Fe centers; exceptions include a series of dinuclear compounds[30−38] and a molecular square.[39] The primary reason for this lack of interest vis-à-vis magnetic materials is the fact that Co and Fe ions in the presence of CN^- ligands typically undergo redox processes to produce diamagnetic Co^{III} and Fe^{II} centers. These compounds have nonetheless attracted attention because of the characteristic metal-to-metal charge transfer (MM′CT) band in the visible region. This offers much promise for designing optically switchable materials,[40−43] as demonstrated by Bernhardt et al., who have reported pronounced color changes in dinuclear Co/Fe complexes as a function of the metal oxidation states.[44] This feature has also been utilized in extended Prussian blue frameworks, where irradiation of the sample with light can be used to tune the magnetic properties. For instance, Hashimoto et al. noted that illumination of the Prussian blue analogue, $K_{0.2}Co_{1.4}[Fe(CN)_6]\cdot 6.9H_2O$, at low temperatures increased the critical ordering temperature of the solid.[13] It has been shown that this is a result of external stimuli initiating a charge-transfer-induced spin transition (CTIST) between diamagnetic low-spin (LS) Co^{III} ($S = 0$) and LS Fe^{II} ($S = 0$) centers to generate a ferromagnetic regime of high-spin (HS) Co^{II} ($S = {}^3/_2$) and LS Fe^{III} ($S = {}^1/_2$) centers.[45] The resultant metastable $Co^{II}_{HS}-NC-Fe^{III}_{LS}$ framework is stabilized by strong cooperativity effects of the extended lattice as well as structural defects, features that are considered to be prerequisite for trapping the photoinduced species. As a result, only a limited number of examples of metal-cyanide solids have been shown to exhibit this photoinduced magnetic behavior, and the CTIST has hitherto been a property exclusive to extended frameworks.[13,45−61]

Scheme 1. Trigonal Bipyramidal Cores of **1**−**4**

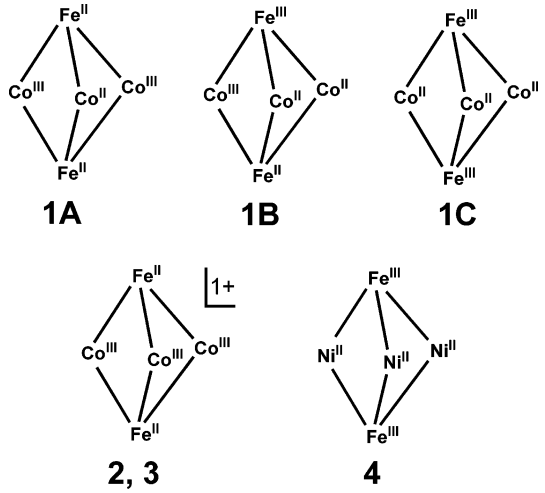

In the vein of exploring new types of Co/Fe cyanide compounds, we recently synthesized a discrete pentanuclear CN^--bridged complex, $\{[Co(tmphen)_2]_3[Fe(CN)_6]_2\}$ (**1**) (tmphen = 3,4,7,8-tetramethyl-1,10-phenanthroline), and demonstrated that the electronic spin state of each metal center is exquisitely sensitive to temperature and/or degree of solvation.[62] A combination of structural, magnetic, and Mössbauer data has been used to support the fact that the red crystalline product exists in the isomeric form $\{Co^{II}_3Fe^{III}_2\}$ **1C** at room temperature and that the molecule is converted to the $\{Co^{III}Co^{II}_2Fe^{III}Fe^{II}\}$ **1B** or $\{Co^{III}_2Co^{II}Fe^{II}_2\}$ **1A** forms at $T < 130$ K (Scheme 1). We rationalize that this process is a result of a CTIST, an unprecedented finding for a Co/Fe complex. In addition to an extensive investigation of the CTIST that occurs in the red crystalline phase, we probe herein the physical properties of a blue solid phase that is produced upon exposure of the red crystals to humidity, and a red solid phase that is obtained upon desolvation. To elucidate the complicated behavior of these three phases of **1**, we also report the properties of two new structurally related, trigonal bipyramidal compounds that are relevant benchmarks for the mixed valence Fe/Co compound **1**. These include $Na\{[Co^{III}(tmphen)_2]_3[Fe^{II}(CN)_6]_2\}(ClO_4)_2$ (**2**), a cationic

(26) Sessoli, R.; Gatteschi, D.; Caneschi, A.; Novak, M. A. *Nature* **1993**, *365*, 141−143.
(27) Sessoli, R.; Tsai, H. L.; Schake, A. R.; Wang, S. Y.; Vincent, J. B.; Folting, K.; Gatteschi, D.; Christou, G.; Hendrickson, D. N. *J. Am. Chem. Soc.* **1993**, *115*, 1804−1816.
(28) Gatteschi, D.; Sessoli, R. *Angew. Chem., Int. Ed.* **2003**, *42*, 268−297.
(29) Christou, G.; Gatteschi, D.; Hendrickson, D. N.; Sessoli, R. *MRS Bull.* **2000**, *25*, 66−71.
(30) Bernhardt, P. V.; Macpherson, B. P.; Martinez, M. *J. Chem. Soc., Dalton Trans.* **2002**, 1435−1441.
(31) Bernhardt, P., V.; Moore, E. G.; Riley, M. J. *Inorg. Chem.* **2001**, *40*, 5799−5805.
(32) Bernhardt, P., V.; Macpherson, B. P.; Martinez, M. *Inorg. Chem.* **2000**, *39*, 5203−5208.
(33) Bernhardt, P. V.; Martinez, M. *Inorg. Chem.* **1999**, *38*, 424.
(34) Zhan, S. Z.; Chen, X. Y.; Meng, Q. J.; Xei, W. *Synth. React. Inorg. Met. -Org. Chem.* **1996**, *26*, 277−284.
(35) Vogler, A.; Kunkely, H. *Phys. Chem. Chem. Phys.* **1975**, *79*, 301−307.
(36) Hester, R. E.; Nour, E. M. *J. Chem. Soc., Dalton Trans.* **1981**, 939−941.
(37) Bagger, S.; Stoltze, P. *Acta Chem. Scand. A* **1983**, *37*, 247−250.
(38) Bagger, S.; Gibson, K. *Acta Chem. Scand.* **1972**, *26*, 3788−3796.
(39) Oshio, H.; Onodera, H.; Tamada, O.; Mizutani, H.; Hikichi, T.; Ito, T. *Chem.—Eur. J.* **2000**, *6*, 2523−2530.
(40) Mortimer, R. J. *Chem. Soc. Rev.* **1997**, *26*, 147−156.
(41) Chang, C.; Ludwig, D.; Bocarsly, A. *Inorg. Chem.* **1998**, *37*, 5467−5473.
(42) Guihery, N.; Durand, G.; Lepetit, M. B. *Chem. Phys.* **1994**, *183*, 45−59.
(43) Harihar, G.; Prabhakara Rao, G. *Sol. Energy Mater.* **1994**, *33*, 499−504.
(44) Bernhardt, P. V.; Bozoglian, F.; Macpherson, B. P.; Martinez, M.; Merbach, A. E.; Gonzalez, G.; Sienra, B. *Inorg. Chem.* **2004**, *43*, 7187−7195.
(45) Sato, O.; Einaga, Y.; Fujishima, A.; Hashimoto, K. *Inorg. Chem.* **1999**, *38*, 4405−4412.
(46) Sato, O.; Einaga, Y.; Iyoda, T.; Fujishima, A.; Hashimoto, K. *J. Electrochem. Soc.* **1997**, *144*, L11−L13.
(47) Bleuzen, A.; Lomenech, C.; Escax, V.; Villain, F.; Varret, F.; Moulin, C. C. D.; Verdaguer, M. *J. Am. Chem. Soc.* **2000**, *122*, 6648−6652.
(48) Moulin, C. C. D.; Villain, F.; Bleuzen, A.; Arrio, M. A.; Sainctavit, P.; Lomenech, C.; Escax, V.; Baudelet, F.; Dartyge, E.; Gallet, J. J.; Verdaguer, M. *J. Am. Chem. Soc.* **2000**, *122*, 6653−6658.
(49) Escax, V.; Bleuzen, A.; Moulin, C. C. D.; Villain, F.; Goujon, A.; Varret, F.; Verdaguer, M. *J. Am. Chem. Soc.* **2001**, *123*, 12536−12543.
(50) Pejakovic, D. A.; Manson, J. L.; Kitamura, C.; Miller, J. S.; Epstein, A. J. *Polyhedron* **2001**, *20*, 1435−1439.
(51) Moore, J. G.; Lochner, E. J.; Ramsey, C.; Dalal, N. S.; Stiegman, A. E. *Angew. Chem., Int. Ed.* **2003**, *42*, 2741−2743.
(52) Ohkoshi, S. I.; Arai, K. I.; Sato, Y.; Hashimoto, K. *Nat. Mater.* **2004**, *3*, 857−861.
(53) Tokoro, H.; Ohkoshi, S. I.; Hashimoto, K. *Appl. Phys. Lett.* **2003**, *82*, 1245−1247.
(54) Shimamoto, N.; Ohkoshi, S.; Sato, O.; Hashimoto, K. *Inorg. Chem.* **2002**, *41*, 678−684.
(55) Gu, Z. Z.; Einaga, Y.; Sato, O.; Fujishima, A.; Hashimoto, K. *J. Solid State Chem.* **2001**, *159*, 336−342.
(56) Ohkoshi, S.; Yorozu, S.; Sato, O.; Iyoda, T.; Fujishima, A.; Hashimoto, K. *Appl. Phys. Lett.* **1997**, *70*, 1040−1042.
(57) Ohkoshi, S.; Machida, N.; Zhong, Z. J.; Hashimoto, K. *Synth. Met.* **2001**, *122*, 523−527.
(58) Ohkoshi, S.; Hashimotoi, K. *J. Am. Chem. Soc.* **1999**, *121*, 10591−10597.
(59) Arimoto, Y.; Ohkoshi, S. i.; Zhong, Z. J.; Seino, H.; Mizobe, Y.; Hashimoto, K. *J. Am. Chem. Soc.* **2003**, *125*, 9240−9241.
(60) Rombaut, G.; Verelst, M.; Golhen, S.; Ouahab, L.; Mathoniere, C.; Kahn, O. *Inorg. Chem. 40*, 1151−1159.
(61) Sato, O. *Acc. Chem. Res.* **2003**, *36*, 692−700.
(62) Berlinguette, C. P.; Dragulescu-Andrasi, A.; Sieber, A.; Galan-Mascaros, J. R.; Guedel, H. U.; Achim, C.; Dunbar, K. R. *J. Am. Chem. Soc.* **2004**, *126*, 6222−6223.

molecular cluster that is the oxidation product of **1**, and the complex $\{[Co^{III}(bpy)_2]_3[Fe^{II}(CN)_6]_2\}[Fe^{III}(CN)_6]_{1/3}$ (**3**). In addition, the previously reported cluster, $\{[Ni^{II}(tmphen)_2]_3[Fe^{III}(CN)_6]_2\}$ (**4**),[63] is revisited to document the physical and structural parameters of bona fide M−NC−Fe clusters.[64]

Experimental Section

Materials. The starting materials $Co(NO_3)_2 \cdot 6H_2O$ and $K_3[Fe(CN)_6]$ were purchased from Fisher Scientific, and the reagents 2,2′-bipyridine (bpy), 3,4,7,8-tetramethyl-1,10-phenanthroline (tmphen), and 18-crown-6 were purchased from Aldrich. The salt $[(18\text{-crown-6})K]_3[Fe(CN)_6]$ was prepared in situ by stirring an excess of $K_3[Fe(CN)_6]$ in a solution of 18-crown-6 in acetonitrile (MeCN). The cluster $\{[Ni(tmphen)_2]_3[Fe(CN)_6]_2\}$ (**4**)$\cdot 14H_2O$[63] and ferrocenium hexaflourophosphate[65] ($[Fc][PF_6]$) were prepared as previously reported.

Syntheses. $\{[Co(tmphen)_2]_3[Fe(CN)_6]_2\}$ **(1):** $Co(NO_3)_2 \cdot 6H_2O$ (100 mg, 0.35 mmol) was dissolved in 60 mL of MeCN and treated with 2 equiv of tmphen (160 mg, 0.70 mmol) dissolved in 20 mL of MeCN. The salt $[(18\text{-crown-6})K]_3[Fe(CN)_6]$ (50 mg, 0.06 mmol) dissolved in 50 mL of MeCN was slowly added to the former solution, and the mixture was immediately filtered and then left to stand undisturbed for 2 days to yield X-ray quality red crystals. Yield = 25 mg (∼34%). A blue solid was obtained from the crystals upon filtration in a humid atmosphere. Anal. Calcd for $C_{108}H_{144}Co_3Fe_2N_{24}O_{24}$ (24 interstitial H_2O molecules): C, 52.92; H, 5.93; N, 13.71; O, 15.67. Found: C, 52.95; H, 5.73; N, 13.81; O, 15.40. ESI-MS (MeOH): *m*/*z* 1009 ($\{H[Co(tmphen)_2]_3[Fe(CN)_6]_2\}^{2+}$) (Figure S1).

$Na\{[Co(tmphen)_2]_3[Fe(CN)_6]_2\}(ClO_4)_2$ **(2):** A sample of **1** (20 mg, 0.01 mmol) was dissolved in 20 mL of MeOH and combined with 1 equiv of $[Fc][PF_6]$ (4 mg, 0.01 mmol) to yield a blue solution. An excess of $NaClO_4$ (10 mg, 0.1 mmol) dissolved in 3 mL of H_2O was subsequently added to the solution, and the reaction mixture was left to stand undisturbed for 2 days to yield X-ray quality blue plates. Yield = 25 mg (∼90%). This product was verified by single-crystal X-ray diffraction techniques.

$\{[Co(bpy)_2]_3[Fe(CN)_6]_2\}[Fe(CN)_6]_{1/3}$ **(3):** A quantity of $Co(NO_3)_2 \cdot 6H_2O$ (140 mg, 0.48 mmol) was dissolved in 160 mL of a MeOH/H_2O mixture (3/5, v:v) and combined with 2 equiv of bpy (150 mg, 0.96 mmol) dissolved in 20 mL of MeOH. The resulting orange solution was then carefully layered on a 180 mL MeOH/H_2O solution (5/13, v:v) of $K_3[Fe(CN)_6]$ (160 mg, 0.50 mmol) to yield a blue solution at the interface. The reaction mixture was left to stand undisturbed for one week to yield X-ray quality dark blue needles. The product was filtered and washed with copius amounts of MeOH, MeCN, acetone, and diethyl ether: Yield = 0.30 g (∼75%). Anal. Calcd for $C_{74}N_{26}H_{76}O_{14}Co_3Fe_{2.33}$ (14 interstitial H_2O molecules): C, 47.78; H, 4.13; N, 19.58; O, 12.25. Found: C, 46.31; H, 4.20; N, 19.27; O, 12.25.

Physical Measurements. Infrared (IR) spectra of the blue solid phase of **1** and compounds **2**−**4** were measured as Nujol mulls placed between KBr plates on a Nicolet 740 FT-IR spectrometer. The IR spectra of the red crystalline and red solid phases of **1** were collected as mineral oil mulls prepared in an inert atmosphere. Optical absorption spectra of the solid phases were recorded on a Fourier transform spectrometer equipped with the appropriate light sources, beam splitters, and detectors (Bruker IFS66). Data on the red crystalline phase were collected in mineral oil, the blue solid was suspended in glycerol, and the red solid in a KBr pellet. Temperatures between 11 and 300 K were achieved with a closed-cycle cryosystem with the sample sitting in He exchange gas (Oxford Instruments CCC 1204). Solution optical absorption spectra were collected on a Shimadzu UV 1601PC spectrophotometer. X-band EPR spectra were collected on a Bruker 300 spectrometer equipped with an Oxford ESR 910 cryostat and a Bruker bimodal cavity. Electrochemical measurements were carried out by using an H−CH Electrochemical Analyzer model 620A. Cyclic voltammetric measurements were performed in MeCN with 0.1 M tetra-*n*-butylammonium hexaflourophosphate ($TBAPF_6$) as the supporting electrolyte. The working electrode was a BAS Pt disk electrode, the reference electrode was Ag/AgCl, and the auxiliary electrode was a Pt wire. The ferrocene couple is at $E_{1/2} = +0.52$ V versus Ag/AgCl under these same conditions.

DC Magnetic susceptibility measurements were carried out with the use of a Quantum Design SQUID magnetometer MPMS-XL at an applied external field of 1000 G in the 2−300 K temperature range. Samples were prepared in gelatin capsules sealed with Kapton tape (Quantum Design). To circumvent solvent loss from the red crystals, liquid eicosane was carefully added to the suspension of crystals in MeCN. The diamagnetic contribution of the capsule, tape, eicosane, and MeCN was determined to be $-3.7(2) \times 10^{-5}$ emu in a 1000 G field over the entire temperature range; the diamagnetic contributions of the cluster and solvent were calculated using Pascal constants.[66]

The ^{57}Fe Mössbauer spectra were collected on constant acceleration instruments over the 1.5−300 K temperature range in applied external fields up to 80 kG. Spectral simulations were generated using WMOSS (WEB Research, Edina, MN), and isomer shifts are reported relative to Fe metal foil at room temperature. Mössbauer samples of red crystals of **1** were prepared by washing the crystals with copious amounts of MeCN to ensure that the crystals remained covered with MeCN at all times. A suspension of crystals in MeCN was placed in a Mössbauer cup and frozen for experiments between 4.2 and 220 K. A sample for room-temperature Mössbauer experiments was prepared in a cup covered with a Teflon lid and sealed with Teflon tape to avoid desolvation during data collection. Visual inspection indicated that the crystals remained wet and maintained their red color for the duration of the data collection. Filtration of the red crystals in a humid atmosphere leads to a blue material that was placed in a Mössbauer cup covered with a lid. The red solid obtained by exposing the blue material to vacuum was placed in a Mössbauer cup in a drybox to prevent exposure to moisture and oxygen. These samples were contained in sealed Mössbauer cups and were not exposed to air during data collection.

Single-Crystal X-ray Diffraction. Single-crystal X-ray data sets were collected on nine different red crystals of $\{[Co(tmphen)_2]_3[Fe(CN)_6]_2\}$ (**1**) at $T = 30(2)$ K (**1**^{a}), 90(2) K (**1**^{b}), 110(2) K (**1**^{c}), 130(2) K (**1**^{d}), 150(2) K (**1**^{e}), 170(2) K (**1**^{f}), 190(2) K (**1**^{g}), 220(2) K (**1**^{h}), and 293(2) K (**1**^{i}); a blue platelet of **2** at $T = 150(2)$ K; and a blue needle of **3** at $T = 110(2)$ K. X-ray data sets for **1**, **2**, and **3** were collected on a Bruker APEX CCD X-ray diffractometer using Mo Kα radiation ($\lambda_\alpha = 0.710\ 73$ Å). Single crystals were immersed in paraffin oil, secured on a nylon loop with Dow Corning silicone grease and placed in a cold $N_{2(g)}$ stream at the appropriate temperature, except for **1**^{i}, which was secured on the tip of a glass fiber with epoxy and measured at 293(2) K. The diffraction patterns for each crystal were indexed using SMART software[67] to obtain the unit cell parameters. The frames were integrated with the Bruker SAINT software package,[68] and the data were corrected for absorption using the program SADABS.[69] The structures were solved and refined using X-SEED,[70] a graphical interface to the SHELX suite of programs.[71] For each crystal, all non-hydrogen atoms were located from the initial Fourier difference map and were refined anisotropically. The hydrogen atoms were placed in calculated

(63) Berlinguette, C. P.; Galan-Mascaros, J. R.; Dunbar, K. R. *Inorg. Chem.* **2003**, *42*, 3416−3422.
(64) Berlinguette, C. P. Ph.D. Dissertation, Texas A&M University, College Station, TX, 2004.
(65) Connelly, N. G.; Geiger, W. E. *Chem. Rev.* **1996**, *96*, 877−910.
(66) Boudreaux, E. A.; Mulay, L. N. *Theory and Applications of Molecular Paramagnetism*; Wiley: New York, 1976; p 512.
(67) Bruker. *SMART Software for Windows NT*; Bruker AXS, Inc.: Madison, WI, 2001.
(68) *Saint, Program for area detector absorption correction*; Siemens Analytical X-ray Instruments: Madison, WI, 1994.
(69) Bruker. *SADABS*; Bruker AXS, Inc.: Madison, WI, 2001.
(70) Barbour, L. J. *J. Supramol. Chem.* **2003**, *1*, 189−191.
(71) Sheldrick, G. *Shelxl-97 Program for Crystal Structure Refinement*; Gottingen, Germany, 1997.

Table 1. Crystallographic Data and Structural Refinement Parameters for Separate Crystals of $\{[Co(tmphen)_2]_3[Fe(CN)_6]_2\}$ (**1**) over the 30−298 K Temperature Range[a]

	(**1**[a])·$9H_2O$	(**1**[c])·$13H_2O$	(**1**[h])·$9H_2O$	(**1**[i])·$6H_2O$
formula	$C_{108}H_{114}Co_3Fe_2N_{24}O_9$	$C_{108}H_{122}Co_3Fe_2N_{24}O_{13}$	$C_{108}H_{112}Co_3Fe_2N_{24}O_8$	$C_{108}H_{108}Co_3Fe_2N_{24}O_6$
T (K)	30(2)	110(2)	220(2)	293(2)
a (Å)	18.94(1)	19.02(1)	19.261(4)	19.04(2)
b (Å)	24.79(2)	25.03(2)	25.123(5)	24.91(3)
c (Å)	24.33(1)	24.65(2)	24.782(5)	24.62(4)
β (deg)	97.77(9)	97.86(2)	97.74(3)	97.64(8)
V (Å^3)	11319(12)	11626(15)	11883(4)	11569(25)
Z	4	4	4	4
fw	2181.71	2252.77	2176.3	2208.67
space group	$P2_1/c$ (No. 14)	$P2_1/c$ (No. 14)	$P2_1/c$ (No. 14)	$P2_1/c$ (No. 14)
crystal system	monoclinic	monoclinic	monoclinic	monoclinic
GOF (F^2)	1.094	1.035	1.034	1.035
$R(F_o)^b$, $R_w(F_o^2)^c$	0.1255, 0.3021	0.0760, 0.2058	0.0765, 0.2234	0.0735, 0.2039

[a] Note: All data were collected using Mo Kα radiation (λ = 0.710 73 Å). [b] $R(F_o) = \Sigma[(F_o - F_o)]/\Sigma(F_o)$. [c] $R_w(F_o^2) = \{\Sigma[w(F_o^2 - F_c^2)^2]/\Sigma[w(F_o^2)^2]\}^{1/2}$.

Table 2. Crystallographic Data and Structural Refinement Parameters for $Na\{[Co(tmphen)_2]_3[Fe(CN)_6]_2\}(ClO_4)_2$ (**2**) and $\{[Co(bpy)_2]_3[Fe(CN)_6]_2\}$ $[Fe(CN)_6]_{1/3}$ (**3**)

	(**2**)·$34H_2O$	(**3**)·$20H_2O$
formula	$C_{108}H_{164}Co_3Fe_2Cl_2O_{42}NaN_{24}$	$C_{74}H_{88}Co_3Fe_{2.33}N_{26}O_{20}$
T (K)	150(2)	110(2)
a (Å)	18.86(3)	18.530(3)
b (Å)	25.22(3)	18.530(3)
c (Å)	29.69(5)	31.483(6)
α (deg)	90	90
β (deg)	97.52(6)	90
γ (deg)	90	120
V (Å^3)	13 400(40)	9362(3)
Z	4	4
fw	2852.98	1968
space group	$P2_1/n$ (No. 14)	$P6_322$ (No. 182)
crystal system	monoclinic	hexagonal
GOF (F^2)	1.011	1.122
$R(F_o)$,[b] $R_w(F_o^2)$[c]	0.0970, 0.2470	0.0699, 0.1963
Flack parameter		0.05(4)

[a] Note: All data were collected using Mo Kα radiation (λ = 0.710 73 Å). [b] $R(F_o) = \Sigma[(F_o - F_o)]/\Sigma(F_o)$. [c] $R_w(F_o^2) = \{\Sigma[w(F_o^2 - F_c^2)^2]/\Sigma[w(F_o^2)^2]\}^{1/2}$.

positions, and their thermal parameters were fixed to be 20% larger than those of the atoms to which they are bound (50% in the case of methyl groups). The crystal parameters and basic information pertaining to the data collection and refinement for crystals **1**−**3** are summarized in Tables 1−2 and S1−S2.

For compounds **1**[a]−**1**[i], the diffraction patterns were each indexed using a primitive monoclinic cell and were solved in the space group $P2_1/c$ (No. 14) based on the systematic absences. The asymmetric unit consists of the pentanuclear cluster and highly disordered interstitial solvent molecules. Data collection at different temperatures could not be carried out on the same crystal because temperature fluctuations compromised the diffraction quality of the crystals. The disordered solvent in the crystals was assigned as H_2O molecules with variable occupancy factors (0.2−1.0), but it should be noted that the presence of MeCN cannot be ruled out and should be expected. The electron density of the interstitial solvent molecules was best refined as 6 to 13 H_2O molecules over the measured temperature range. A full analysis of the void space in the unit cell was carried out using PLATON.[72] The SQUEEZE option was used to treat the weak reflection data for each crystal and to correct for the disordered solvent. This process improved the refinement parameters for each crystal slightly but did not significantly affect the metrical parameters (Table S2).

The diffraction pattern of a blue platelet (0.47 × 0.38 × 0.03 mm^3) of $Na\{[Co(tmphen)_2]_3[Fe(CN)_6]_2\}(ClO_4)_2$(**2**)·$34H_2O$ was indexed using a primitive monoclinic cell and was solved in the space group $P2_1/n$ (No. 14) based on the systematic absences. The asymmetric unit consists of the pentanuclear cluster, one Na^+ ion, two $(ClO_4)^-$ ions, and 34 interstitial H_2O solvent molecules.The crystal system for $\{[Co(bpy)_2]_3[Fe(CN)_6]_2\}[Fe(CN)_6]_{1/3}$ (**3**)·$20H_2O$ is hexagonal, and the space group is $P6_322$ (No. 182). The highly disordered counterion, $[Fe(CN)_6]^{3-}$, was refined to a site occupancy of 1/3 based on electron density and consideration of charge balance (vide infra). The interstices of the crystal are occupied by solvent molecules assigned as disordered H_2O molecules, with occupancy factors from 1.0 to 0.20.

(72) Spek, A. L. *PLATON. Program for Crystal Structure Results Analysis*; Utrecht, The Netherlands, 2002.

Scheme 2. Routes to the Three Solid-State Phases of **1**

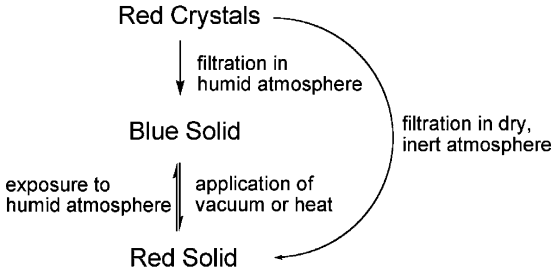

Results and Discussion

Synthesis and Molecular Structure of $\{[Co(tmphen)_2]_3[Fe(CN)_6]_2\}$ (1). The successful isolation of pure crystalline phases of trigonal bipyramidal, cyanide-bridged compounds depends on several factors, namely, solvent, the nature of the coligands, and the counterion. The bidentate ligand 3,4,7,8-tetramethyl-1,10-phenanthroline, for instance, enhances the solubility of complexes in organic media thereby circumventing the rapid formation of undesirable polymeric phases that is typical for metal-cyanide chemistry. Indeed, this ligand has been shown to favor the formation of pentanuclear trigonal bipyramidal clusters containing various metals in appreciable yields.[25,63] Given the success of this approach, we used $\{Co(tmphen)_2\}^{2+}$ and $[Fe(CN)_6]^{3-}$ as precursors to successfully generate red crystals of the pentanuclear cluster, $\{[Co(tmphen)_2]_3[Fe(CN)_6]_2\}$ (**1**).

Over the course of our investigation of **1**, it was noted that handling of samples led to dramatic color changes depending on the temperature and/or the presence of solvent (Scheme 2). For example, filtration of red crystals of **1** in a humid atmosphere leads to a blue solid, whereas filtration in a dry, inert environment produces a red solid. The dramatic color changes associated with the manipulation of **1** are related to its exquisite sensitivity to solvent content. With the caveat that a precise determination of the solvent content for the red crystals is

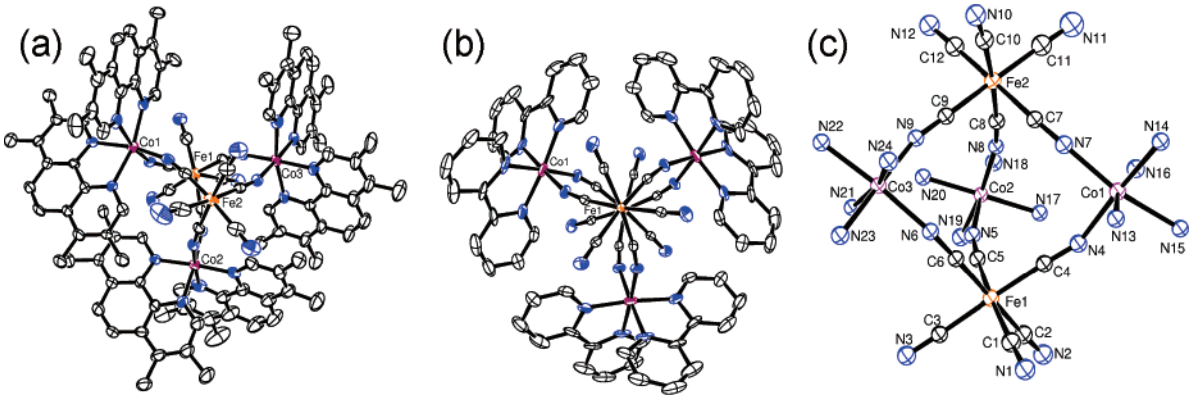

Figure 1. Thermal ellipsoid plots drawn at the 50% probability level for: (a) **1**[a] and (b) the complex cation of **3**; (c) the numbering scheme of the cores for **1**−**3**.

experimentally difficult due to rapid changes in solvent content upon removal of the crystals from the mother liquor, single-crystal X-ray crystallography supports a range of 6 to 13 H_2O molecules per cluster of **1** for the red crystalline phase. Elemental analyses indicate a higher H_2O content for the blue material (ca. 24 H_2O molecules/cluster **1**) and a lower H_2O content for the red solid phase (ca. 2 H_2O molecules/cluster **1**).[73] A red solid is also formed by exposing the blue solid to higher temperatures or vacuum, but in this case the color change from blue to red is reversible; i.e., the red solid is converted back to a blue solid upon exposure to a humid environment. Furthermore, cooling a suspension of red crystals in MeCN to $T = 77$ K leads to a color change from red to blue. This observation suggests that the metal centers in **1** undergo an electronic transformation as a function of temperature.

A variable-temperature X-ray diffraction study over the 30−293 K temperature range was carried out on nine separate crystals (**1**[a]−**1**[i]). The space group and unit cell parameters did not exhibit any significant changes over the entire temperature range (Table 1). The $\{[Co(tmphen)_2]_3[Fe(CN)_6]_2\}$ (**1**) cluster consists of three octahedral $\{Co(tmphen)_2\}^{n+}$ units situated in the equatorial plane of a trigonal bipyramid that are bridged through CN^- ligands to two octahedral $[Fe(CN)_6]^{n-}$ units that occupy the apical positions of the bipyramid (Figure 1a). The three $\{Co(tmphen)_2\}^{n+}$ moieties within one cluster exhibit identical chiralities (all Λ or all Δ), but both homochiral cluster enantiomers are present in the crystal leading to the centrosymmetric space group, $P2_1/c$. The enantiomers exhibit $\pi-\pi$ interactions (3.47 Å) between the tmphen ligands coordinated to the Co(1) centers, which provide the shortest *inter*molecular M···M contacts of ca. 8.3 Å (Figure S2); there are no $\pi-\pi$ contacts between the tmphen ligands bound to the Co(2) and Co(3) sites.

It is difficult to assign oxidation states of the metal ions in **1** based on metrical parameters because the complex contains Fe and Co ions, both of which can be divalent or trivalent and can adopt LS or HS electronic configurations. The Fe ions in **1** are most likely LS due to the strong ligand field created by the CN^- ligands, but it remains difficult to assign oxidation state because the Fe−CN distances in polynuclear systems containing $[Fe(CN)_6]^{3-,4-}$ units are typically insensitive to oxidation state.[21,32,39,63,74,75] Indeed in the present case, the Fe−C bond lengths remain relatively constant between 30 K (1.866(9)−1.92(1) Å) and room temperature (1.88(1)−1.94(1) Å) (Table 3), despite the change in oxidation state of the Fe ions over this temperature range (vida infra). Similarly, negligible differences were observed in the ∠C−Fe−C bond angles, with the maximum measured difference between 30 and 293 K being 2.2° (Table 3).

Although temperature does not have a notable effect on the cell parameters or on the Fe−C metrical parameters, it influences the geometry of the Co ions significantly (Table 3). The Co centers are bound to the nitrogen end of the bridging CN^- ligand, which can stabilize LS Co^{III} ($S = 0$), LS Co^{II} ($S = {}^1/_2$), or HS Co^{II} ($S = {}^3/_2$) electronic configurations. The possibility of HS Co^{III} ions being stabilized in this ligand environment was dismissed because the only known examples of this situation are $[CoF_6]^{3-}$,[76] $[CoF_3(OH_2)_3]$,[76] and the Klaui complexes.[77−80] The three possible electronic configurations for $Co^{II/III}$ ions can generally be distinguished by structural data; e.g., Co−N_{bpy} bond distances typically follow the trend: LS Co^{III} (∼1.9 Å) < LS Co^{II} (∼2.0 Å) < HS Co^{II} (∼2.1 Å).[30,32,33,75,81]

The Co−N bond distances for all three Co centers of complex **1** over the 220−293 K temperature range are ∼2.1 Å (Table 3), which are indicative of HS Co^{II}. To preserve the neutral charge of **1**, the oxidation states of the two Fe sites in the cluster can therefore be indirectly assigned as Fe^{III}. Thus, the red crystalline phase of **1** at temperatures above 220 K can be described as $\{Co^{II}_3Fe^{III}_2\}$ **1C**. The Co(1)−N bond distances remain relatively constant as the temperature is lowered, whereas the Co(2) and Co(3) centers exhibit a significant decrease in bond lengths, reaching values between 1.947(6) Å and 2.037(6) Å at $T = 30$ K (Figure 2). The ∠N−Co−N values follow the same trend as the bond lengths; namely, there are no significant changes between 30 K and room temperature (0.2° to 2.8°), but the values at the other two Co sites change significantly by up to 6.3° and 8.5° for the Co(2) and Co(3)

(73) Weak diffraction powder patterns of the blue and red solids precluded structural investigations of these phases.

(74) Bernhardt, P. V.; Bozoglian, F.; Macpherson, B. P.; Martinez, M.; Gonzalez, G.; Sienra, B. *Eur. J. Inorg. Chem.* **2003**, 2512−2518.
(75) Lescouezec, R.; Vaissermann, J.; Ruiz-Perez, C.; Lloret, F.; Carrasco, R.; Julve, M.; Verdaguer, M.; Dromzee, Y.; Gatteschi, D.; Wernsdorfer, W. *Angew. Chem., Int. Ed.* **2003**, *42*, 1483−1486.
(76) Cotton, F. A.; Wilkinson, G.; Bochmann, M.; Murillo, C. *Advanced Inorganic Chemistry*, 6th ed.; Wiley Interscience: New York, 1998.
(77) Eberspach, W.; Elmurr, N.; Klaui, W. *Angew. Chem., Int. Ed.* **1982**, *21*, 915−916.
(78) Klaui, W. *J. Chem. Soc., Chem. Commun.* **1979**, 700.
(79) Klaui, W.; Eberspach, W.; Gutlich, P. *Inorg. Chem.* **1987**, *26*, 3977−3982.
(80) Lejay, J.; Jansen, A. G. M.; Wyder, P.; Bronger, W.; Klaui, W. *Phys. Rev. B* **1991**, *43*, 8196−8198.

Table 3. Selected Bond Distances (Å) and Angles (deg) for **1** at Selected Temperatures, **2**, and **3**

	1					
connectivity	(30 K)	(110 K)	(220 K)	(293 K)	**2**	**3**
Co(1)−N(4)	1.999(7)	2.028(8)	2.059(7)	2.031(9)	1.85(1)	1.879(3)
Co(1)−N(7)	2.062(7)	2.069(10)	2.099(9)	2.042(9)	1.89(2)	1.879(3)
Co(1)−N(13)	2.106(7)	2.139(8)	2.154(7)	2.135(8)	1.91(1)	1.919(3)
Co(1)−N(14)	2.130(6)	2.167(8)	2.154(7)	2.122(8)	1.93(1)	1.949(4)
Co(1)−N(15)	2.157(7)	2.177(8)	2.177(7)	2.133(7)	1.93(1)	1.949(4)
Co(1)−N(16)	2.068(8)	2.136(7)	2.151(7)	2.146(7)	1.94(1)	1.919(3)
Co(2)−N(5)	1.924(8)	1.915(9)	2.040(9)	2.042(9)	1.86(1)	1.879(3)
Co(2)−N(8)	1.947(6)	1.948(9)	2.035(8)	2.035(9)	1.86(1)	1.879(3)
Co(2)−N(17)	2.027(7)	1.987(7)	2.110(7)	2.131(8)	1.90(1)	1.919(3)
Co(2)−N(18)	1.948(8)	1.995(8)	2.125(7)	2.145(8)	1.91(1)	1.949(4)
Co(2)−N(19)	1.972(8)	1.979(9)	2.124(9)	2.135(9)	1.92(1)	1.949(4)
Co(2)−N(20)	1.987(7)	1.982(8)	2.103(7)	2.086(8)	1.92(1)	1.919(3)
Co(3)−N(6)	1.977(7)	1.956(9)	2.056(8)	2.087(9)	1.85(1)	1.879(3)
Co(3)−N(9)	1.920(7)	1.939(8)	2.010(8)	2.016(9)	1.86(1)	1.879(3)
Co(3)−N(21)	2.010(6)	2.016(7)	2.114(6)	2.115(8)	1.92(1)	1.919(3)
Co(3)−N(22)	2.037(6)	2.038(7)	2.144(7)	2.165(8)	1.92(1)	1.949(4)
Co(3)−N(23)	1.965(7)	1.997(7)	2.114(7)	2.136(8)	1.94(1)	1.949(4)
Co(3)−N(24)	1.987(7)	1.992(8)	2.116(7)	2.103(8)	1.96(1)	1.919(3)
Fe(1)−C(1)	1.92(1)	1.95(1)	1.93(1)	1.90(2)	1.88(2)	1.914(5)
Fe(1)−C(2)	1.86(1)	1.93(1)	1.92(1)	1.92(1)	1.89(2)	1.914(5)
Fe(1)−C(3)	1.91(1)	1.93(1)	1.95(1)	1.93(1)	1.90(2)	1.914(5)
Fe(1)−C(4)	1.908(9)	1.90(1)	1.942(9)	1.92(1)	1.91(2)	1.901(4)
Fe(1)−C(5)	1.89(1)	1.90(1)	1.93(1)	1.91(1)	1.92(2)	1.901(4)
Fe(1)−C(6)	1.901(8)	1.94(1)	1.93(1)	1.89(1)	1.94(2)	1.901(4)
Fe(2)−C(7)	1.879(8)	1.90(1)	1.93(1)	1.94(1)	1.86(2)	1.914(5)
Fe(2)−C(8)	1.882(8)	1.90(1)	1.92(1)	1.91(1)	1.87(2)	1.914(5)
Fe(2)−C(9)	1.866(9)	1.89(1)	1.91(1)	1.91(1)	1.88(2)	1.914(5)
Fe(2)−C(10)	1.898(9)	1.92(1)	1.92(1)	1.88(1)	1.89(2)	1.901(4)
Fe(2)−C(11)	1.92(1)	1.97(1)	1.92(1)	1.95(1)	1.90(2)	1.901(4)
Fe(2)−C(12)	1.86(1)	1.91(1)	1.89(1)	1.88(1)	1.91(2)	1.901(4)
N(4)−Co(1)−N(13)	91.6(3)	91.1(3)	90.8(3)	90.5(3)	90.3(5)	88.8(2)
N(4)−Co(1)−N(14)	167.7(3)	167.9(3)	167.7(3)	167.7(3)	175.9(5)	177.2(1)
N(4)−Co(1)−N(7)	92.0(3)	91.3(3)	90.3(3)	91.7(3)	90.3(5)	88.5(2)
N(5)−Co(2)−N(18)	172.0(3)	171.3(3)	167.1(3)	165.9(3)	174.7(5)	177.2(1)
N(5)−Co(2)−N(19)	89.3(3)	89.8(3)	90.5(3)	89.3(3)	89.6(4)	88.8(2)
N(8)−Co(2)−N(5)	93.9(3)	93.0(3)	94.3(3)	96.1(3)	90.9(5)	88.5(2)
N(6)−Co(3)−N(22)	175.2(2)	174.8(3)	172.1(3)	170.1(3)	176.0(5)	177.2(1)
N(6)−Co(3)−N(23)	88.5(3)	88.2(3)	88.5(3)	88.3(3)	90.7(4)	88.8(2)
N(9)−Co(3)−N(6)	90.9(2)	90.8(3)	91.2(3)	92.3(3)	91.3(4)	88.5(2)
C(1)−Fe(1)−C(2)	84.1(4)	87.9(4)	88.1(4)	88.6(4)	88.8(6)	90.6(2)
C(1)−Fe(1)−C(4)	88.5(4)	87.6(4)	88.6(3)	88.8(4)	90.9(5)	86.6(2)
C(1)−Fe(1)−C(5)	174.8(4)	175.3(4)	176.8(3)	176.5(4)	178.8(6)	176.9(2)
C(7)−Fe(2)−C(11)	86.9(4)	86.6(5)	87.9(4)	88.0(4)	88.3(5)	86.6(2)
C(9)−Fe(2)−C(11)	176.9(4)	176.2(4)	177.6(4)	177.6(4)	177.6(5)	176.9(2)

sites, respectively. These data indicate that Co(1) is HS Co^{II} over the entire temperature range, while the Co(2) and Co(3) centers undergo an electronic structure transformation between 220 and 110 K. The intercluster $\pi-\pi$ interactions between the tmphen ligands coordinated to the Co(1) centers, which are absent for the ligands bound to the Co(2) and Co(3) centers, may explain this unique behavior at the Co(1) site.

Below 110 K, the Co(2)−N and Co(3)−N bond distances are intermediate between LS Co^{III} and HS Co^{II}. The possibility of a HS → LS transition at the Co^{II} ion was ruled out on the basis of the changes in oxidation state of the Fe centers (to be discussed in the Mössbauer and Magnetism sections). As a result, the intermediate Co−N bond lengths are due to either static disorder in the crystal leading to a superposition of LS Co^{III} and HS Co^{II} centers, or to electron delocalization between the Co^{II} and Co^{III} ions. The latter is an unlikely hypothesis, however, given that there are no direct orbital pathways between the Co ions. The most likely scenarios are that an equimolar mixture of clusters **1A** and **1C** exist in the crystal lattice or that clusters **1B** are present in the crystal in different orientations (Scheme 3). It is difficult to discern experimentally which of these two situations holds true for the title compound, but it is clear that an electronic transformation affects the Co(2) and Co(3) ions as the temperature increases.

Synthesis and Molecular Structure of Na{[Co(tmphen)$_2$]$_3$[Fe(CN)$_6$]$_2$}(ClO$_4$)$_2$ (2). Addition of [Fc][PF_6] to a green solution of **1** in MeOH generates a color change to a blue solution. Subsequent addition of an aqueous solution of $NaClO_4$ leads to the formation of dark blue platelike crystals upon standing in air for one week. These crystals were determined by single-crystal X-ray crystallography to represent the one-electron oxidized form of **1**, Na{[Co(tmphen)$_2$]$_3$[Fe(CN)$_6$]$_2$}(ClO$_4$)$_2$(**2**)·34H_2O (space group = $P2_1/n$). The asymmetric unit contains the cluster {[Co(tmphen)$_2$]$_3$[Fe(CN)$_6$]$_2$}$^+$, a disordered Na^+ ion situated near the terminal N atoms of the cluster, two $(ClO_4)^-$ anions located in close proximity to the {Co(tmphen)$_3$}$^{3+}$ ions, and disordered interstitial H_2O molecules. The cluster in **2** adopts the same geometry as that in **1**, with three {Co(tmphen)$_2$}$^{3+}$ units and two [Fe^{II}(CN)$_6$]$^{4-}$ units forming a trigonal bipyramidal geometry. The Co−N distances are significantly shorter (1.85(1)−1.96(2) Å) (Table 3) than the corresponding distances in **1**, an indication that the cluster

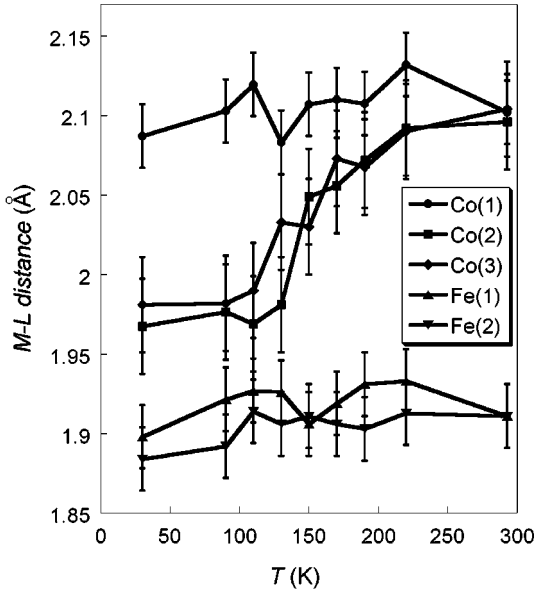

Figure 2. Temperature dependence of M−L distances (Å) in red crystals of **1** (vertical bars correspond to standard deviation).

Scheme 3. Static Disorder of Co^{II} and Co^{III} Sites Due to Superposition of (a) **1B** in Different Orientations; or (b) **1A** and **1C**

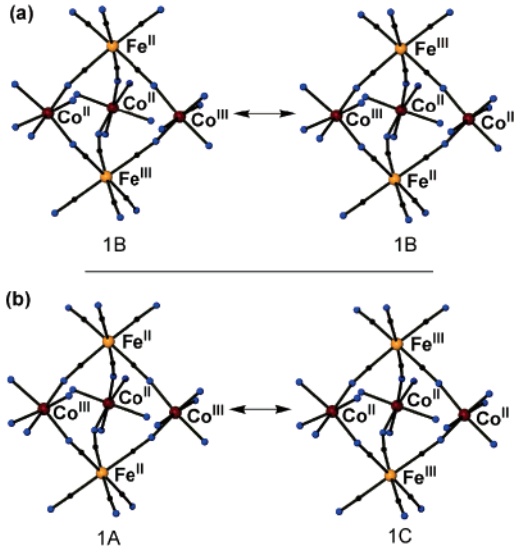

contains three LS Co^{III} ions. Based on charge balance considerations, the oxidation states of the two Fe ions (Fe−C = 1.87(2)−1.94(2) Å) are assigned as LS Fe^{II}. In contrast to **1**, color changes as a function of temperature were not observed for **2**.

Synthesis and Molecular Structure of $\{[Co(bpy)_2]_3[Fe(CN)_6]_2\}[Fe(CN)_6]_{1/3}$ (3). The reaction of $\{Co(bpy)_2\}^{2+}$ with $K_3[Fe(CN)_6]$ in a mixture of water and MeOH yields blue needlelike crystals of $\{[Co(bpy)_2]_3[Fe(CN)_6]_2\}[Fe(CN)_6]_{1/3}$ (**3**) in high yield. Compound **3** crystallizes in the chiral hexagonal space group $P6_322$ (No. 182), with two independent $\{[Co(bpy)_2]_3[Fe(CN)_6]_2\}^+$ cations per asymmetric unit each at one-sixth occupancy and one-third of a $[Fe(CN)_6]^{3-}$ counterion unit refined to a total occupancy of one-third (Figures S3 and S4). The complex cation in **3** adopts a trigonal bipyramidal geometry with three $\{Co(bpy)_2\}^{3+}$ units situated in the equatorial plane and connected to two apical $[Fe(CN)_6]^{4-}$ units via the N end of three *fac* CN^- ligands (Figure 1b). The Co−N distances are in the range 1.863(4) Å to 1.949(4) Å (Table 3), which is in accord with those for LS Co^{III}−N distances. The Fe−C distances vary from 1.901(4) Å to 1.918(5) Å, which is consistent with LS Fe^{II} as required by charge balance considerations, magnetism, and Mössbauer data (vide infra). The unit cell contains two crystallographically inequivalent clusters with Co centers of opposite chirality; i.e., the three Co centers are Λ, Λ, Λ in one cluster and Δ, Δ, Δ in the other. Both clusters exhibit idealized D_3 symmetry with the 3-fold axis passing through the Fe centers and the three perpendicular 2-fold axes passing through each of the three Co centers. The clusters pack in the crystal in a fashion that facilitates intercluster $\pi-\pi$ interactions between the bpy ligands coordinated to all of the Co centers. The spaces between the clusters (~3500 $Å^3$) are occupied by interstitial H_2O molecules and the $[Fe(CN)_6]^{3-}$ counterion, which is located near the special position (1/3, 2/3, 1/4) at 1/3 occupancy (Figure S4).[82]

^{57}Fe Mössbauer Spectroscopy. Iron ions in $[Fe(CN)_6]^{n-}$ (n = 3, 4) units adopt LS configurations and exhibit comparable isomer shifts (δ) over a broad temperature range (e.g., between 0.00 and −0.20 mm/s at 4.2 K, relative to Fe metal at room temperature) rendering it difficult to discriminate the Fe oxidation states based only on isomer shift. In contrast, the quadrupole splitting (ΔE_Q) of Fe^{II} sites is relatively small (<0.2 mm/s) as compared to that of Fe^{III} sites (>0.26 mm/s). Furthermore, Mössbauer data collected in an applied magnetic field allows for the distinction between the slow-relaxing paramagnetic LS Fe^{III} ($S = {}^1/_2$) ions, which have magnetically split Mössbauer spectra due to hyperfine interactions, and diamagnetic LS Fe^{II} ions, whose spectra are split only by nuclear Zeeman interactions.

As shown in Scheme 1, the Fe sites in each of the three phases of compound **1** adopt either +2 or +3 oxidation states. To elucidate the oxidation state of these sites in each of these phases, we collected Mössbauer spectra in an applied magnetic field of 0−80 kG over the 2−300 K temperature range and have compared the Mössbauer parameters obtained for **1** with those for **3** and **4**, which have a well-defined, unambiguous valence assignment.

Compound **3** contains octahedral LS Fe^{II} ions in the complex cation $\{[Co^{III}(bpy)_2]_3[Fe^{II}(CN)_6]_2\}^+$ and an octahedral LS Fe^{III} site in the counterion $[Fe^{III}(CN)_6]^{3-}$ generating a stoichiometric Fe^{II}/Fe^{III} ratio of 6:1. The 4.2 K Mössbauer spectrum of this complex reveals the presence of a line spectrum attributed to the LS Fe^{II} ions in the complex cation, $\{[Co^{III}(bpy)_2]_3[Fe^{II}(CN)_6]_2\}^+$, and an underlying broad paramagnetic feature attributed to the presence of LS Fe^{III} ions in the counterion $[Fe^{III}(CN)_6]^{3-}$ (Figure 3). The experimentally determined ratio between the absorption of Fe^{II} and Fe^{III} is 5.7:1 (LS Fe^{II} = 85(3)%; LS Fe^{III} = 15(3)%), which is very close to 6:1 calculated based on the stoichiometry of compound **3** (Table 4).

Mössbauer spectra of red crystals of **1** suspended in MeCN were recorded at temperatures between 4.2 and 220 K, in applied

(81) Sieber, R.; Decurtins, S.; Stoeckli-Evans, H.; Wilson, C.; Yufit, D.; Howard, J. A. K.; Capelli, S. C.; Hauser, A. *Chem.—Eur. J.* **2000**, *6*, 361−368.
(82) To verify the identity of the counterion, compound **3** was also prepared using the precursor "$[Co(bpy)_2][ClO_4]_2$" rather than "$[Co(bpy)_2][NO_3]_2$" which led to the isolation of blue needle crystals that were determined by X-ray diffraction techniques to be identical to those obtained by the synthetic route described in the Experimental Section. The XPS data collected on the new crystals ruled out the presence of Cl^- providing further support that the counterion is, indeed, $[Fe(CN)_6]^{3-}$.

Table 4. Mössbauer Parameters for Selected Fe Types in the Three Solid-State Phases of **1**, **3**, and **4**, and Representative Prussian-Blue Analogues

compound	Fe type	T (K)	δ (mm/s)	ΔE_Q (mm/s)	ratio (Fe^{II}/Fe^{III})
1, red crystals	Fe^{II}	4.2	0.02	0.2	40:60−50:50[a] 70:30[b]
	Fe^{III}	220	−0.08	0.61	0:100[a] 20:80[b]
1, blue solid	Fe^{II}	4.2	0.02	0.2	100:0
	Fe^{II}	293	−0.06	0.15	>75:<25
1, red solid	Fe^{III}	20	−0.04	1.40	<15:>85
	Fe^{III}	220	−0.09	1.00	<15:>85
3	Fe^{II}	4.2	0.02	0.2	85:15
4	Fe^{III}	150	−0.06	0.79	0:100
$Co^{II}_{1.5}[Fe^{III}(CN)_6]\cdot 6H_2O$[45]	Fe^{III}	293	−0.17	0.61	0:100
$Rb_{0.66}Co^{II}_{0.84}Co^{III}_{0.41}[Fe^{II}(CN)_6]\cdot 4.3H_2O$[45]	Fe^{II}	293	−0.08	0.16	100:0

[a] Large crystals. [b] Small crystals.

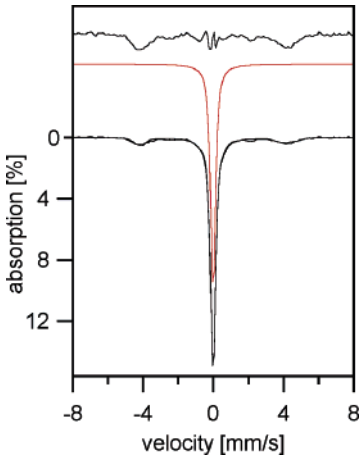

Figure 3. Mössbauer spectrum for $\{[Co^{III}(bpy)_2]_3[Fe^{II}(CN)_6]_2\}[Fe^{III}(CN)_6]_{0.33}$ (**3**) at $T = 4.2$ K. The contributions of LS Fe^{II} (shown in red) and LS Fe^{III} sites present in the sample are depicted separately above the experimental spectrum.

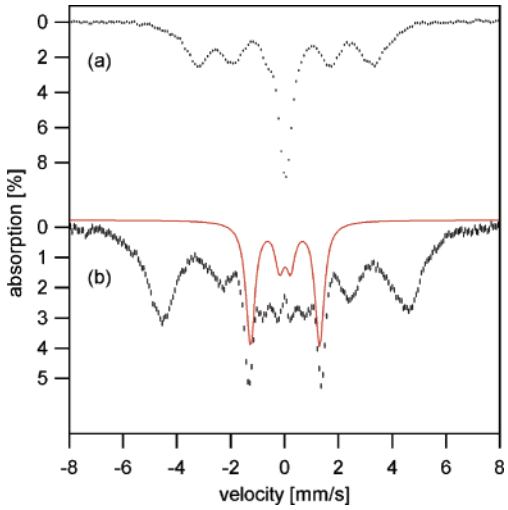

Figure 4. Mössbauer spectra of red crystals of **1** recorded at $T = 4.2$ K in applied fields of 0.45 kG (a) and 80 kG (b). The spectral simulation (solid line) for the Fe^{II} site (40%) is shown separately, above the high field spectrum.

fields up to 80 kG. Five samples from independent preparations were investigated: the average crystal size from four preparations was large (ca. $1 \times 1 \times 1$ mm^3) and gave similar Mössbauer spectra at all temperatures. Analysis of the spectra of the four samples indicates that each sample contains two distinct types of Fe sites. The 4.2 K spectra consist of a line spectrum characteristic of LS Fe^{II} accompanied by broad paramagnetic features spread over the velocity range between −4 and +4 mm s^{-1}, which are indicative of intermediate relaxation and are attributed to LS Fe^{III} sites (Figure 4a). A 80 kG Mössbauer spectrum confirmed that the line spectrum is due to a diamagnetic LS Fe^{II} site with parameters $\delta = 0.02$ mm s^{-1}, $\Delta E_Q = 0.2$ mm s^{-1}, and asymmetry parameter $\eta = 0$ (Figure 4b).[83] Thus, the 4.2 K Mössbauer spectra indicate that the four samples containing the large crystals contain both LS Fe^{II} and LS Fe^{III} sites, with the LS Fe^{II} content varying between 40% and 50%; variable-temperature Mössbauer spectra indicate that the sample composition remains constant up to 110 K. Based on these data, it is concluded that the large crystals of **1** below 110 K consist of a mixture of LS Fe^{II} and LS Fe^{III} ions in an ∼1:1 ratio.

The 4.2 K Mössbauer data collected for small crystals of **1** obtained from a fifth preparation revealed a higher LS Fe^{II} content (70(3)%) than that observed for large crystals. This observation further supports the sensitivity of compound **1** to extrinsic factors and, as explained below, provides an opportunity to obtain Mössbauer parameters for the Fe^{III} sites in the sample as a function of temperature, which was not possible for samples that have an ∼1:1 mixture of Fe^{II} and Fe^{III}. The broad, magnetically split features observed at 4.2 K for LS Fe^{III} collapse at temperatures above 30 K into a quadrupole doublet distinguished by a shoulder (marked by arrows in Figure 5 and S5), a feature that is observed up to 190 K. A Fourier transform procedure was applied to the spectra to remove the line width contribution of the ^{57}Co(Rh) source.[84] In the transformed spectra at temperatures below 150 K, the left-side shoulder belongs to a quadrupole doublet with δ and ΔE_Q values (Table 5 and Figure S5) that are typical for octahedral LS Fe^{III} sites with cyanide coordination.[45,85] For example, the 150 K Mössbauer spectrum of $\{[Ni(tmphen)_2]_3[Fe(CN)_6]_2\}$ (**4**),[63] which is isostructural to **1** and contains only LS Fe^{III}, consists of a doublet with δ and ΔE_Q of −0.06 and 0.79 mm/s, respectively. Analysis of the spectra and their Fourier transforms for the small crystals of **1** afforded Mössbauer parameters for the LS Fe^{III} sites at each

(83) It is important to note that, while the low-field Mössbauer spectrum could be simulated also with ΔE_Q values smaller than 0.2 mm s^{-1}, the high field spectrum can only be simulated with $\Delta E_Q = 0.2$ mm s^{-1}.

(84) Dibar-Ure, C.; Flinn, P. A. In *Mössbauer Effect Methodology*; Gruverman, I. J., Ed. Plenium Press: New York, 1971; pp 245−262.

(85) Greenwood, N. N.; Gibb, T. C. *Mossbauer Spectroscopy*; Chapman and Hall: London, 1971.

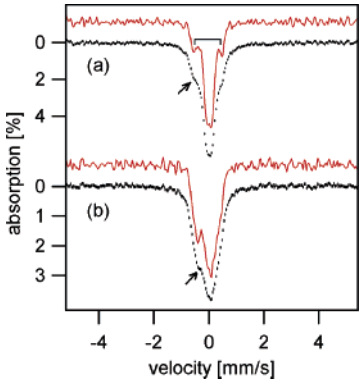

Figure 5. Mössbauer spectra and Fourier transforms of the spectra (shown in red) for a sample containing small red crystals of **1** recorded at 110 K (a) and 190 K (b). Arrows mark the shoulder that is due to the left line of the doublet for LS Fe^{III}. Bracket marks the quadrupole doublet for LS Fe^{III}.

Table 5. Mössbauer Parameters for Fe^{III} Ions in Small Red Crystals of **1**

T (K)	δ (mm s^{-1})	ΔE_Q (mm s^{-1})
30	−0.02	0.98
110	−0.04	0.79
150	−0.05	0.73
190	−0.06	0.67

temperature (Table 5). The isomer shift becomes more negative with increasing temperature because of the second-order Doppler shift, while ΔE_Q decreases from 0.98 mm/s at $T = 30$ K to 0.61 mm/s at $T = 220$ K, a feature that has been noted previously for LS Fe^{III}.[85] The spectra collected at 30 and 110 K are identical and indicate that the sample composition is unaltered up to 110 K. Above 110 K, however, the Fe^{II}/Fe^{III} ratio decreases substantially, with the LS Fe^{II} ions comprising only ∼20% of the sample at $T = 220$ K (Figure 6b). By using the Mössbauer parameters obtained for LS Fe^{III} in the small red crystals (Table 5), the high-temperature spectra of the four samples of large crystals were analyzed. For these samples, the Fe^{II}/Fe^{III} ratio was also shown to decrease above 110 K, with the 220 K Mössbauer spectra revealing a well-resolved doublet consistent with the presence of exclusively LS Fe^{III} ions ($\delta \approx -0.06$ mm s^{-1}, $\Delta E_Q \approx 0.61$ mm s^{-1}) (Figure 6a).

The Mössbauer data indicate that crystals of **1** contain a mixture of Fe^{II} and Fe^{III} sites below 110 K, which is compatible with either the presence of **1B**, or a mixture of **1A** and **1C**. Data recorded at temperatures above 110 K reveal an increase in the Fe^{III} content irrespective of the Fe^{II}/Fe^{III} ratio below 110 K (Figure 7). These observations provide incontrovertible evidence that both the small and large red crystals undergo a CTIST that favors the conversion to **1C** at higher temperatures. One scenario that is compatible with the Mössbauer data for red crystals of **1** is that, below 110 K, large crystals contain a mixture of forms **1A** and **1C** in a ∼1:1 ratio, whereas small crystals have a higher content of **1A** (Figure 7). Above 110 K, the Fe^{III} content of the sample increases, which indicates a CTIST of **1A** to **1B** or, more likely, **1C**. An alternative explanation is that, below 110 K, large crystals contain **1B** clusters (which have the same valence distribution as a 1:1 mixture of **1A** and **1C**). In this scenario, the small crystals would contain some **1A** clusters besides **1B** in order to explain the higher Fe^{II} content in the sample. Above 110 K, however, the

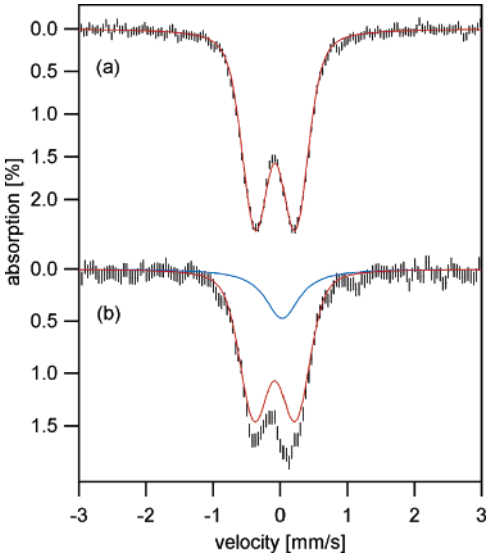

Figure 6. Mössbauer spectra of the large (a) and small (b) red crystals of **1** from two independent preparations recorded at $T = 220$ K. The red solid lines represent a quadrupole doublet corresponding to the parameters, $\delta = -0.08$ mm/s and $\Delta E_Q = 0.61$ mm/s. The contribution of the Fe^{III} sites is 80% in part b; the blue line represents the contribution of Fe^{II} (20%).

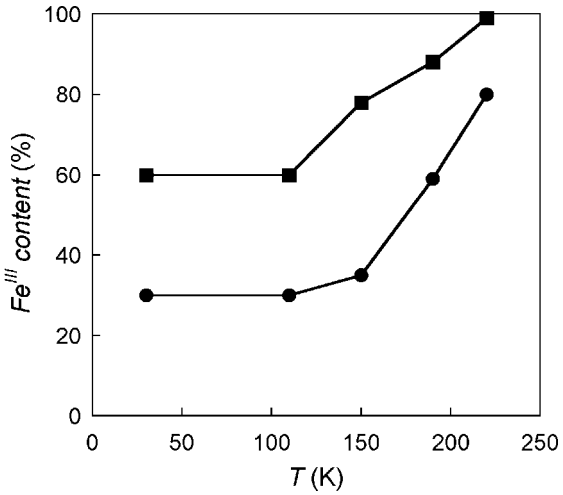

Figure 7. Temperature dependence of the LS Fe^{III} content for two samples of small (●) and large (■) red crystals of **1**. Solid line is merely to guide the eye.

increased Fe^{III} content of the samples is also due to a CTIST, which converts **1B** to **1C**.

The Mössbauer spectra of the blue solid phase of **1** consists of a single absorption line at all temperatures between 4.2 and 293 K (spectra not shown), consistent with the presence of LS Fe^{II}. A spectrum recorded on the same sample in an applied magnetic field of 70 kG at 4.2 K confirmed that all Fe sites present in the sample are diamagnetic;[62] thus, the blue solid form of **1** is exclusively $\{Co^{III}_2Co^{II}Fe^{II}_2\}$ **1A** at low temperatures. Mössbauer data collected at 293 K also revealed a single line spectrum typical of LS Fe^{II}. However, it is important to note that this spectrum may conceal the presence of a small quadrupole doublet that originates from a minority of LS Fe^{III} sites (<25%) due to the relatively similar isomer shifts for LS Fe^{II} and LS Fe^{III} ions in a CN^- coordination environment. Thus, the Mössbauer data of the blue solid at room temperature indicate that it contains form **1A** and allows for the possibility that a minority of the clusters are **1B** or **1C**.

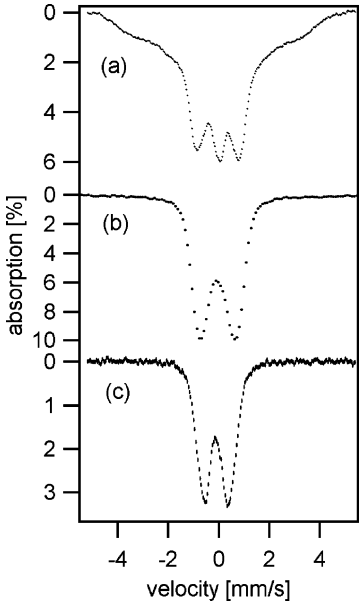

Figure 8. Mössbauer spectra of the red solid of **1** after 10 days under vacuum recorded at $T = 4.2$ K (a), 20 K (b), and 220 K (c) ($H = 0$).

Exposure of the blue solid form of **1** to vacuum (10^{-3} Torr) produces a color change to red within seconds. Mössbauer spectra of samples exposed to vacuum for 1, 5, and 10 days indicate that the duration of exposure to vacuum does not affect the sample composition at high temperatures, but it does have an effect on the relaxation rate of the electronic spin at low temperatures (Figures S6 and S7). For the sake of brevity, only the Mössbauer spectra recorded for a sample exposed to vacuum for 10 days are discussed here.[86] The broad features of the 1.5 K (not shown) and 4.2 K (Figure 8a) spectra indicate an intermediate relaxation process. The 20 K Mössbauer spectrum (Figure 8b) consists of a broad quadrupole doublet ($\Delta E_Q = 1.4$ mm/s; $\delta = -0.04$ mm/s) characteristic of LS Fe^{III} sites. It is important to note that the spectrum may conceal a single-line spectrum arising from the presence of up to 15% LS Fe^{II} sites ($\Delta E_Q = 0.2$ mm/s; $\delta = 0.02$ mm/s). Data collected at 220 K also reveal a quadrupole doublet ($\delta = -0.09$ mm/s; $\Delta E_Q = 1.0$ mm/s) that is consistent with LS Fe^{III} centers (Figure 8c). The average isomer shift of the quadrupole doublet does not vary with temperature between 20 and 293 K (other than by the expected second-order Doppler effect), and we conclude that the average valence of the Fe sites in the sample does not change; i.e., Fe^{III} constitutes >85% of the Fe sites over the entire temperature range. Therefore, the major component of the red solid phase of **1** is best described as $\{Co^{II}{}_3Fe^{III}{}_2\}$ (**1C**) over the entire temperature range investigated.

Mössbauer and EPR Spectroscopy of Compound 1 in Solution. The obvious influence of the solvent content on the properties of **1** in the solid state prompted us to examine its properties in solution. A Mössbauer spectrum collected for a frozen solution of **1** in methanol (spectrum not shown) indicates the presence of LS Fe^{II} sites, exclusively. Thus, compound **1** exists in solution as $\{Co^{II}Co^{III}{}_2Fe^{II}{}_2\}$ **1A** and contains one HS Co^{II} ($S = {}^3/_2$) ion. A perpendicular ($\mathbf{B_1} \perp \mathbf{B}$) mode X-band EPR spectrum was recorded at 15 K on a 1 mM sample obtained by dissolving the red solid phase of **1** in MeOH under anaerobic

(86) Spectra collected on samples that were placed under vacuum for various time intervals are submitted as Supporting Information.

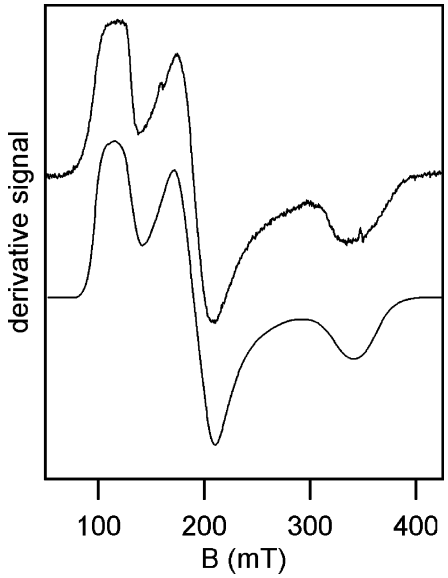

Figure 9. X-band EPR spectrum of a 1 mM solution of **1** in MeOH. Simulation for one $S = {}^3/_2$ species (lower curve) was generated using the spin Hamiltonian given in eq 1 with fine and hyperfine parameters given in the text (experimental conditions: $T = 15$ K; microwave frequency = 9.65 GHz; microwave power = 0.02 mW; modulation amplitude = 9.43 G).

conditions (Figure 9). The apparent *g*-values (5.85, 3.62, and 2.02) determined from this spectrum are typical for HS Co^{II} sites: *g*-values for the tetragonally distorted octahedral complex, $[Co(acac)_2(6\text{-Mequin})]$, are 5.83, 3.92, and 1.98,[87] and for [Co-(triphenylphosphine-oxide)$_2$], which contains a four-coordinate Co^{II} ion with C_2 symmetry, they are 5.91, 3.64, and 2.11.[88] Thus, EPR spectroscopy confirms the presence of HS Co^{II} in **1** in solution.

HS Co^{II} ions with octahedral coordination have a $^4T_1$ ground state, the orbital degeneracy of which is removed if the symmetry is lowered and leads to either a doublet and a singlet, or three singlet orbital states. Since the local symmetry of Co^{II} in the *cis*-$[Co(tmphen)_2(NC)_2]$ moiety is C_2, it can have a nondegenerate orbital ground state. If the ground state is orbitally nondegenerate and well separated from the excited states, spin−orbit coupling leads to four energy levels, the energy of which can be obtained using the spin Hamiltonian:

$$H = \beta S \cdot \tilde{g} \cdot B + D\left(S_z^2 - \frac{5}{4}\right) + E(S_x^2 - S_y^2) + AS \cdot I \quad (1)$$

where D and E describe zero-field splitting, $\tilde{g}$ is the g-tensor, and A is the nuclear hyperfine constant for ^{59}Co ($S = {}^7/_2$, 100%). The EPR spectrum is simulated in Figure 9 using software written by Hendrich et al.[89] based on this Hamiltonian with a large positive D and $E/D = 0.186$, $g_1 = 2.53$, $g_2 = 2.42$, $g_3 = 2.22$, and $A = 148$ G. The large intrinsic *g*-values indicate an important orbital contribution, which would potentially render the use of the spin Hamiltonian invalid. At this end, a detailed

(87) Bencini, A.; Benelli, C.; Gatteschi, D.; Zanchini, C. *Inorg. Chem.* **1980**, *19*, 3027−3030.
(88) Makinen, M. W.; Kuo, L. C.; Yim, M. B.; Wells, G. B.; Fukuyama, J. M.; Kim, J. E. *J. Am. Chem. Soc.* **1985**, *107*, 5245−5255.
(89) Hendrich, M. P.; Petasis, D.; Arciero, D. M.; Hooper, A. B. *J. Am. Chem. Soc.* **2001**, *123*, 2997−3005.

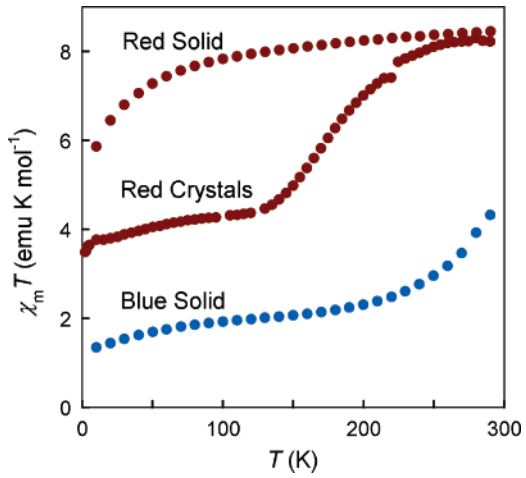

Figure 10. Plot of $\chi_m T$ versus T for the three solid-state phases of **1**: red crystals, blue and red solid (H = 1000 G).

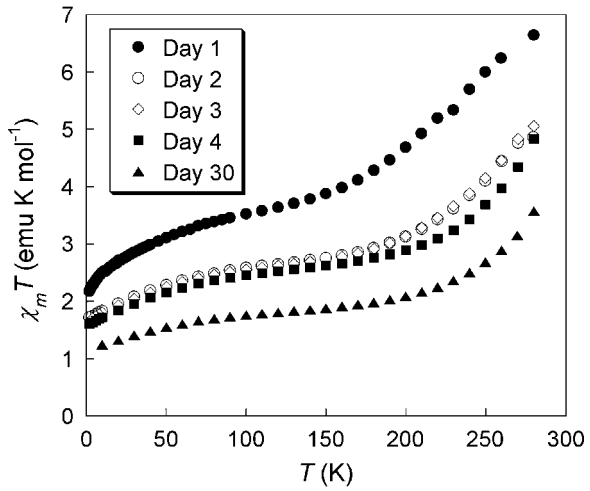

Figure 11. Plot of $\chi_m T$ versus T for the blue solid of **1** collected as a function of exposure time to ambient conditions (H = 1000 G).

analysis of the EPR spectra using AOM and DFT calculations and including spin−orbit coupling is in progress.[90]

Magnetic Properties of {[Co(tmphen)$_2$]$_3$[Fe(CN)$_6$]$_2$} (1). Variable temperature magnetic susceptibility data were collected on the red crystalline, blue solid and red solid phases of **1**.[90] The $\chi_m T$ product for the red crystals decreases from 8.3 emu K mol^{-1} at room temperature to 4.4 emu K mol^{-1} at T = 130 K, followed by a gradual decrease to 3.3 emu K mol^{-1} at T = 10 K (Figure 10). The room temperature value is higher than the spin-only value of 6.375 emu K mol^{-1} (g = 2.00) calculated for the {Co$^{II}_3$Fe$^{III}_2$} **1C** configuration. This result is not unexpected, however, in light of the significant orbital contribution expected for both the HS Co^{II} (S = $^3/_2$) and LS Fe^{III} (S = $^1/_2$) ions. Given the fact that the room temperature $\chi_m T$ products for K$_3$[Fe(CN)$_6$] and HS Co^{II} ions are 0.6 emu K mol^{-1} and 2.0−3.2 emu K mol^{-1},[81,92] respectively, the room temperature value of 8.3 emu K mol^{-1} is in good agreement with the sum of the experimental values for three HS Co^{II} ions and two LS Fe^{III} ions. The behavior of $\chi_m T$ at T < 130 K is in agreement with the presence of either a 1:1 mixture of **1A** and **1C**, or **1B**. There was no evidence of thermal hysteresis when the temperature was cycled over the 2−290 K range at rates of 0.1−10.0 K/min.

Magnetic susceptibility measurements on the blue solid phase obtained immediately after filtration revealed that the $\chi_m T$ product increases gradually from 2.12 emu K mol^{-1} at 2 K to 3.88 emu K mol^{-1} at 150 K, followed by a sharper increase to 6.64 emu K mol^{-1} at 280 K (Figure 10). It is interesting to note that the magnetic behavior of the blue solid of **1** exhibits a time dependence that is presumably related to the quantity of H$_2$O in the sample (Figure 11). The $\chi_m T$ product of the blue solid immediately after extraction from the mother liquor is higher than the $\chi_m T$ values obtained after >1 day. In fact, the susceptibility of blue samples declines steadily and reaches a value corresponding to one HS Co^{II} ion/cluster only after the sample is kept in air for approximately 1 month. The magnetic behavior of the solid after 30 days is consistent with the presence of **1A** at lower temperatures. The divergence of $\chi_m T$ from the value expected for a single HS Co^{II} ion above 150 K can be attributed to a CTIST that leads to a conversion to **1C**. This behavior is in agreement with the Mössbauer results for the blue solid.

Magnetic susceptibility measurements on the blue solid at T > 280 K show a sharp increase in $\chi_m T$ due to desolvation of the blue solid phase. Resolvation is not possible due to the vacuum of the SQUID chamber,[93] and the $\chi_m T$ product measured upon cooling does not reproduce the values measured in warming mode but is comparable to that of the red solid obtained by pumping on the blue solid (see below). Finally, there was no evidence of thermal hysteresis when the temperature was cycled over the 2−280 K range at rates of 0.1−10.0 K/min for the blue solid.

The $\chi_m T$ product of the red solid phase of **1** obtained after exposure to vacuum for 10 days exhibits a steady decrease from 8.3 emu K mol^{-1} at 350 K to 7.8 emu K mol^{-1} at 100 K, followed by a relatively sharp decrease down to 5.86 emu K mol^{-1} at 2 K (Figure 10). The magnetic behavior over the 2−350 K range is reversible, and there is no evidence of thermal hysteresis. The $\chi_m T$ value at room temperature is the same as the value for the red crystals, indicating the presence of three HS Co^{II} ions and two LS Fe^{III} ions (**1C**). The decrease in $\chi_m T$ as the temperature is lowered is predominantly due to the orbital contribution of the HS Co^{II} and LS Fe^{III} centers down to 50 K. Below this temperature, a number of additional factors can contribute to the decreasing trend of the magnetic data, namely, a partial conversion of **1C** to **1B** and/or **1A**, and weak antiferromagnetic interactions within the cluster. It should be mentioned that Lescouëzec et al. have observed ferromagnetic coupling in an Fe(III)−CN−Co(II) double zigzag chain compound,[75,94] which, based on DFT calculations, was attributed to the near orthogonality of the orbitals in which the unpaired electrons of the metal ions reside. DFT calculations aimed at

(90) Dragulescu-Andrasi, A.; Achim, C.; Berlinguette, C. P.; Dunbar, K. R. Unpublished work.
(91) Measurements on the red crystals were carried out by placing an MeCN suspension of the crystals in a gelatin capsule and coating it with eicosane to prevent MeCN evaporation in the vacuum atmosphere of the SQUID chamber. The layer of MeCN prevented contact of the sample with the warm eicosane (mp 34 °C). To properly fit the data, it was necessary to measure the sample and solvent without eicosane at T < 220 K (the mp of MeCN).
(92) Konar, S.; Mukherjee, P. S.; Drew Michael, G. B.; Ribas, J.; Ray, C. N. *Inorg. Chem. 42*, 2545−2552.
(93) The blue and red solid phases can be produced reversibly by exposure to humidity/vacuum.
(94) Toma, L. M.; Lescouezec, R.; Lloret, F.; Julve, M.; Vaissermann, J.; Verdaguer, M. *Chem. Commun.* **2003**, 1850−1851.

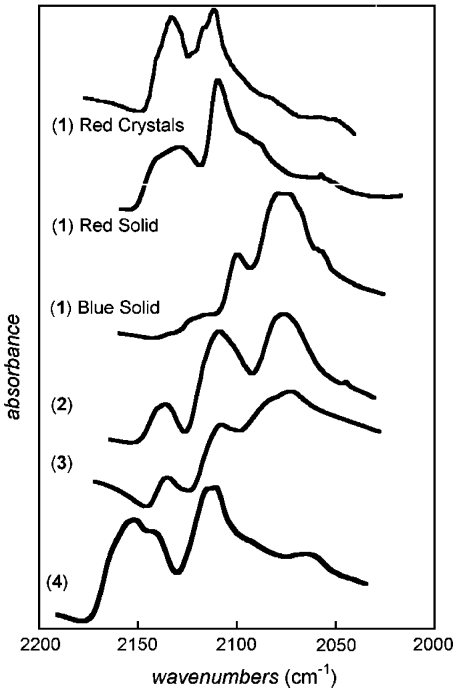

Figure 12. IR spectra for compounds **1**−**4** in the υ_{CN-} region.

elucidating the electronic structure of the metal sites in compound **1** and at evaluating the exchange coupling pathways in the cluster are currently underway in our laboratories.[90]

The $\chi_m T$ product for $\{[Co(bpy)_2]_3[Fe(CN)_6]_2\}[Fe(CN)_6]_{1/3}$(**3**) (Figure S8) exhibits a gradual decrease from ∼0.49 emu K mol^{-1} at 300 K to 0.18 emu K mol^{-1} at 2 K. As the complex cation contains only diamagnetic LS Co^{III} and LS Fe^{II} ions, the paramagnetism is attributed to the counterion, $[Fe(CN)_6]^{3-}$, with the decreasing trend of $\chi_m T$ being attributed to appreciable orbital contributions characteristic for LS Fe^{III} ($S = {}^1/_2$) ions.

The magnetic behavior of $\{[Ni(tmphen)_2]_3[Fe(CN)_6]_2\}$(**4**), which is isostructural to **1**, indicates that the three Ni^{II} ($S = 1$) ions are ferromagnetically coupled to the two LS Fe^{III} ions and that intercluster interactions are not operative down to 2 K due to the large intermolecular M···M distances. The intercluster distances in **1** are comparable to those in **4**, thus the intermolecular interactions are also expected to be negligible for the red crystalline phase of compound **1**. The effects of exposure to vacuum for long periods of time, however, may lead to reduced intermolecular M···M distances rendering intermolecular interactions possible at low temperatures.

Infrared Spectroscopy. Solid-state infrared (IR) spectra in the υ_{CN-} region (1950−2250 cm^{-1}) were recorded for the three solid phases of compound **1** and compounds **2**−**4** at room temperature (Figure 12). We note that the exposure of the red solid phase to moisture could not be completely avoided during sample handling, and thus the sample may have contained a minority of the blue form by the end of data collection. It is also worth noting that compounds **1**−**4** exhibit broad bands due to the presence of crystallographically inequivalent CN^- ligands in each cluster.

The stretching modes observed in the IR spectra of compounds **1**−**4** were assigned based on comparison with benchmark compounds, which allows for conclusions to be made regarding the oxidation state of the metal centers in these clusters. The υ_{CN-} values for $K_3[Fe^{III}(CN)_6]$ and $K_4[Fe^{II}(CN)_6]$ occur at 2115 and 2065 cm^{-1}, respectively, and are generally shifted to higher energies when the CN^- ligand bridges two metal centers. The υ_{CN-} modes for bridging CN^- in Fe/Co systems generally follow the trends:[12,14,35−37,57]

$$2085-2103\,cm^{-1} \qquad Fe^{II}-CN-Co^{II}{}_{HS}$$

$$2116-2133\,cm^{-1} \qquad Fe^{II}-CN-Co^{III}{}_{LS}$$

$$2153-2169\,cm^{-1} \qquad Fe^{III}-CN-Co^{II}{}_{HS}$$

Compounds **2** and **3** both exhibit a band at 2065 cm^{-1} assigned to the $Fe^{II}-CN_{terminal}$ mode and a band at 2137 cm^{-1} attributed to the $Fe^{II}-CN-Co^{III}{}_{LS}$ framework. The signal at 2105 cm^{-1} for **3** is assigned to the $Fe^{III}-CN_{terminal}$ mode in the $[Fe(CN)_6]^{3-}$ counteranion. Compound **4** exhibits a band at 2115 cm^{-1}, attributed to the $Fe^{III}-CN_{terminal}$ mode, and a broad band at 2150 cm^{-1}, assigned to the $Fe^{III}-CN-Ni^{II}$ framework.[63]

The red crystalline and red solid phases of **1** exhibit similar spectra, with two distinct features at 2110 and 2140 cm^{-1}, and bear a striking resemblance to the IR spectrum of complex **4** (Figure 12). The band at 2110 cm^{-1} is attributed to the stretching mode of terminal CN^- ligands coordinated to $Fe^{III}{}_{LS}$ ions, while the higher energy stretch is assigned to $Fe^{III}-CN-Co^{II}{}_{HS}$. Therefore, the IR spectra support the conclusion that at room temperature, the red crystalline and solid phases of **1** are in the **1C** form and contain a $\{Co^{II}{}_3Fe^{III}{}_2\}$ core.

The spectrum of the blue phase of **1** exhibits three IR bands at 2060, 2090, and 2130 cm^{-1} and resembles those of compounds **2** and **3**. The 2060 cm^{-1} band is assigned to the $Fe^{II}{}_{LS}-CN_{terminal}$ mode, whereas the high-energy stretches are attributed to bridging CN^- in $Fe^{II}{}_{LS}-CN-Co^{III}{}_{HS}$ and $Fe^{II}{}_{LS}-CN-Co^{II}{}_{HS}$ frameworks. Thus, the IR spectrum confirms the formulation of the blue solid phase as **1A**.

Although the υ_{CN-} region does not necessarily exhibit systematic changes in frequency with C−N bond lengths,[39] the valence assignment of the metal centers in this IR study is consistent with the different structures of the blue and red solid phases of **1** as determined by X-ray, Mössbauer, and magnetic experiments.

Optical Absorption Spectroscopy. Optical absorption spectroscopy has been extensively used to characterize complexes that exhibit different valence forms because the d−d transitions and charge-transfer bands of such complexes are sensitive to the valence formulation of the compound. Examples of optical transitions that have been assigned in cyanide-bridged Fe/Co systems include the MM′CT ($Fe^{II} \rightarrow Co^{III}$) band at 17 000 cm^{-1} (550 nm) for a thin film of $K_{0.4}Co_{1.3}[Fe(CN)_6]\cdot 5H_2O$,[95] which contains an $Fe^{II}{}_{LS}-CN-Co^{III}{}_{LS}$ framework. Similar transitions have been observed at 25 316 cm^{-1} (395 nm) and 17 700 cm^{-1} (565 nm) in $[(NC)_5Fe^{II}-CN-Co^{III}(CN)_5]^{6-}$ and $[(NC)_5Fe^{II}-CN-Co^{III}(edta)]^{6-}$, respectively.[36,37] More recently, it has been shown that a series of discrete cyanide-bridged $Fe^{II}-Co^{III}$ complexes with cyanide coordination at the Fe^{II} site and saturated amine or amine−thioether coordination at the Co^{III} site exhibit MM′CT ($Fe^{II} \rightarrow Co^{III}$) bands at 17 500 and 19 600 cm^{-1}, respectively.[74] Finally, the complex $Rb_{0.66}Co^{III}{}_{0.84}Co^{II}{}_{0.41}$-$Fe^{II}(CN)_6$],[45] which exhibits an MM′CT ($Fe^{II} \rightarrow Co^{III}$) band at 18 180 cm^{-1} (550 nm), undergoes a CTIST upon illumination

(95) Sato, O.; Einaga, Y.; Iyoda, T.; Fujishima, A.; Hashimoto, K. *J. Phys. Chem. B* **1997**, *101*, 3903−3905.

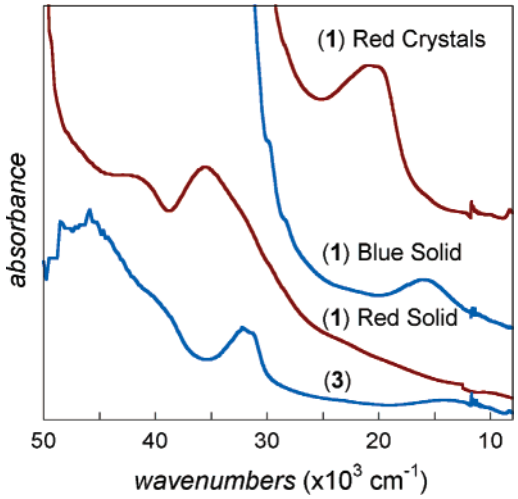

Figure 13. Solid-state UV−vis absorption spectra for the three solid phases of **1** and **3**. (Note: The noisy spectral region at ca. 12 000 cm^{-1} is due to detector change; the data are truncated when light scattering is predominant at high energy.)

to generate an Fe^{III}−CN−Co^{II} framework. Upon this transformation, this band shows a decreased intensity and blue shift to ~16 700 cm^{-1}. To summarize, MM′CT ($Fe^{II} \rightarrow Co^{III}$) bands typically fall in the range 17 000−26 000 cm^{-1}, while MM′CT ($Co^{II} \rightarrow Fe^{III}$) bands are likely to be found at lower energies.

The solid-state UV−vis spectrum of the blue crystals of $\{[Co^{III}(bpy)_2]_3[Fe^{II}(CN)_6]_2\}[Fe(CN)_6]_{1/3}$ (**3**) at 293 K (Figure 13) reveals an intense transition at 32 300 cm^{-1} (309 nm) assigned to MLCT ($Fe^{II} \rightarrow CN^-$) transition[30] and a band at 14 100 cm^{-1} (600 nm) that is assigned to a MM′CT ($Fe^{II} \rightarrow Co^{III}$) transition.[97] The energy of the latter band is lower than those observed for comparable Co/Fe clusters, which exhibit electronic transitions in the 17 000−26 000 cm^{-1} energy range.[17]

Solid-state spectra were recorded for the three phases of **1** at room temperature (Figure 13). The spectra for the red crystals and the blue solid are dominated in the visible range by broad MM′CT transitions at 21 050 and 14 925 cm^{-1}, respectively. The band observed for the blue material exhibits an energy close to that observed for the ($Fe^{II} \rightarrow Co^{III}$) MM′CT bands in **3** (i.e., 14 100 cm^{-1}), while the higher energy band observed for the red crystals is attributed to a $Fe^{II} \rightarrow Co^{III}$ MM′CT. The relationship between the position of the $Fe^{II} \rightarrow Co^{III}$ and $Co^{II} \rightarrow Fe^{III}$ MM′CT bands for the blue solid and red crystal forms of **1**, respectively, can be correlated with the band observed before illumination for $Rb_{0.66}Co_{1.25}[Fe(CN)_6]\cdot 4.3H_2O$, and with the changes observed after illumination for the same compound.[45] The intense band at 35 000 cm^{-1} corresponds to an MLCT band for the $[Fe(CN)_6]^{3-}$ unit in the red solid of **1**.[96,97] Thus, the UV−vis spectra lend further support to the conclusion that the blue solid consists predominantly of the **1A** form of the cluster, and the red crystals correspond to the **1C** form at room temperature. Variable-temperature data did not reveal significant spectral changes, an observation that can be ascribed to the fact the samples are immersed in oil or glycerol rather than MeCN, further highlighting the influence of environmental factors for driving the CTIST.

(96) Lever, A. B. P. *Inorganic Electronic Spectroscopy*; Elsevier: New York, 1968.
(97) The spectrum of the red solid form of **1** does not reveal a band in the visible range due to the fact that the sample prepared in the KBr pellet was too dilute.

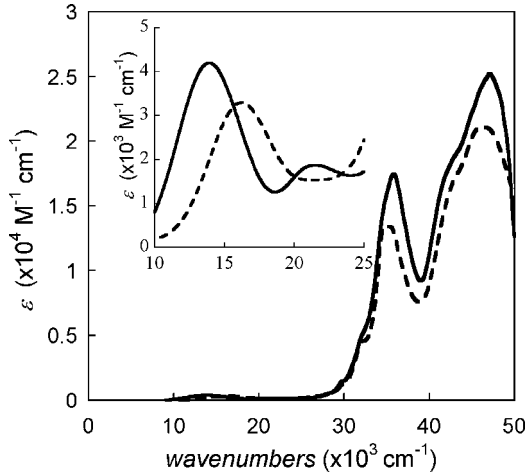

Figure 14. UV−vis absorption spectrum for **1** in dry methanol before (solid line) and after (dashed line) treatment with [Fc][PF_6]. Inset: expanded region in the 10 000−25 000 cm^{-1} range.

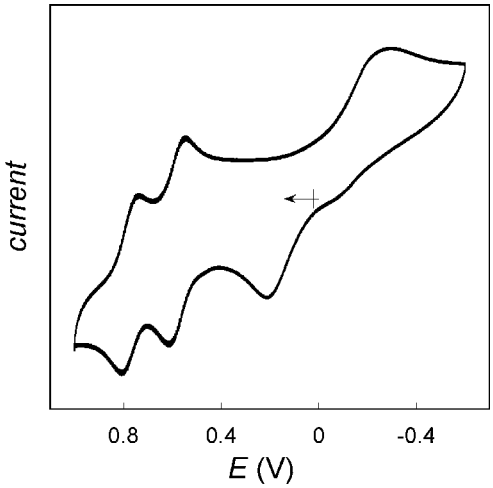

Figure 15. Cyclic voltammogram for compound **1** in 0.1 M $NaClO_4$/MeOH at a Pt disk electrode versus Ag/AgCl.

A green solution of **1** for electronic spectral measurements was prepared by dissolving a sample of the red solid in dry MeOH under inert conditions. The UV−vis spectrum (Figure 14) shows two intense bands in the visible range at 14 700 cm^{-1} (3000 M^{-1} cm^{-1}) and 22 025 cm^{-1} (1500 M^{-1} cm^{-1}). The 14 700 cm^{-1} band is similar to the MM′CT bands observed for the blue form of **1** in solid state and for the MM′CT band of **3**. Therefore, this band is assigned to an MM′CT ($Fe^{II} \rightarrow Co^{III}$) and supports the hypothesis that the cluster adopts the configuration **1A** in solution. The transition observed at 22 025 cm^{-1} is assigned to d−d transitions at the HS Co^{II} site. This assignment was confirmed by the fact that oxidation of **1** with [Fc][PF_6] to **2**, which has a $\{Co_3^{III}Fe_2^{II}\}$ core, leads to disappearance of this band.

Electrochemistry. Electrochemical studies of **1** were carried out in anhydrous MeOH (Figure 15). In addition to the two reversible redox events at $E_{1/2} = +0.59$ V and $E_{1/2} = +0.78$ V, attributed to the oxidation of each of the Fe^{II} centers to Fe^{III} (Scheme 4a), there are several processes that straddle zero potential. These overlapping reduction waves ($E_{p,c} \approx -0.3$ V) and associated oxidation waves ($E_{p,a} \approx +0.2$ V) correspond to redox events at the Co sites that are difficult to resolve. The two reversible $Fe^{II/III}$ couples at 0.59 and 0.78 V are shifted to

Scheme 4. Redox Events for $\{Co^{III}_2Co^{II}Fe^{II}_2\}$ **1** Dissolved in Anhydrous MeOH[a]

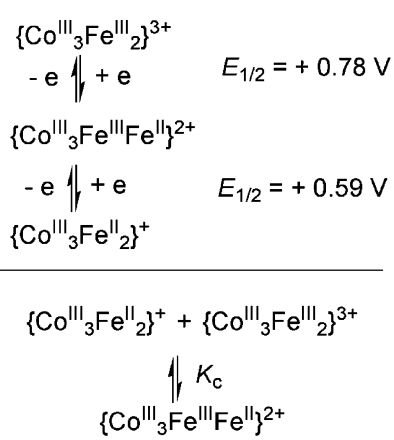

[a] (a) Two reversible 1 e^- $Fe^{II/III}$ redox processes and (b) equation representing the comproportionation constant (K_c) of the species present in solution

higher potentials relative to the experimenally determined value of $E_{1/2} = +0.49$ V for $[18\text{-C-6-K}]_3[Fe(CN)_6]$. This is a result of the bridging Co^{III} ions stabilizing the Fe^{II} centers, a feature consistent with the electrochemical behavior of related Co/Fe compounds.[30,32,33,39,74] The observed peak separation of the two $Fe^{II/III}$ couples ($\Delta E_{1/2} = +0.19$ V) indicates a moderate stability for the dicationic complex $\{Co^{III}_3Fe^{III}Fe^{II}\}^{2+}$, corresponding to a comproportionation constant (K_c) of 2×10^3 (Scheme 4b). In summary, the electrochemical behavior of compound **1** dissolved in MeOH is interpreted as a sequence of the five-step redox process depicted in Scheme 5.

Conclusions

This study provides incontrovertible evidence that compound **1** undergoes a charge-transfer-induced spin transition that is exquisitely sensitive to temperature and degree of solvation. We have determined that there are three distinct phases of **1** in the solid state denoted as the red crystalline, blue solid, and red solid phases. At room temperature, the red crystalline and solid phases are best described by the formulation $\{Co^{II}_3Fe^{III}_2\}$ **1C**. As the temperature is lowered, the crystals undergo a relatively sharp CTIST down to 130 K, whereas the red solid retains its electronic state. At temperatures below 100 K, Mössbauer spectroscopy indicates the presence of LS Fe^{II} and LS Fe^{III} ions in the red crystals, which supports the existence of **1B** or a mixture of **1A** and **1C**. The magnetic susceptibility measurements support this scenario: the room temperature $\chi_m T$ value is in agreement with the presence of three HS Co^{II} and two LS Fe^{III} ions per cluster, and the $\chi_m T$ product below 100 K corresponds to one paramagnetic LS Fe^{III} and two HS Co^{II} sites per cluster. These experimental results converge on the fact that a temperature-dependent intramolecular CTIST between the Fe and Co centers occurs in the red crystals of **1**. In this process, the LS Co^{III} ions are reduced to HS Co^{II} with the concomitant oxidation of the LS Fe^{II} ions to LS Fe^{III}.

Prior to this work, a CTIST had been observed in Co/Fe thin films of the Prussian blue solids,[13] and 2D cyanide arrays,[59] upon irradiation at low temperatures. The effect of light on these systems has been the subject of numerous mechanistic studies,[13,45,54] and it has been found that the transformation is due to a conversion of the diamagnetic $Co^{III}_{LS}-NC-Fe^{II}_{LS}$ framework to a metastable ferromagnetic $Co^{II}_{HS}-NC-Fe^{III}_{LS}$ structure.[45,54] The metastable state is stabilized by the change in Co−N bond distances when the LS Co^{III} centers undergo a charge transfer to form HS Co^{II} centers, which is then trapped in the extended lattice. Taking this point into consideration, the CTIST observed in **1** is unexpected considering that the discrete cluster is not involved in an extended covalent network. Given that other known Co/Fe compounds do not exhibit this behavior, it is not immediately obvious what factors allow compound **1** to exhibit this property. Nonetheless, the significantly different behaviors of the three solid state phases of **1** make it clear that the solvent content plays an important role for determining the temperature range where the CTIST occurs.

While we have learned in the course of this investigation how to convert some of the solid state forms of **1** into each other by exposing them to solvent or vacuum (e.g., the red crystals and red solid transform to blue solid when exposed to humidity; the blue form and red crystals transform into the red solid when exposed to vacuum), we cannot explain the role of the solvent in molecular detail. The influence of solvent on the electronic structure of mixed-valence complexes has been well documented. For instance, single crystals of the complex $(Et_4N)[Fe_2(salmp)_2]$ isolated from MeCN are valence localized up to 300 K as is the complex in solution, but desolvated samples undergo a localization-to-delocalization transition on the Mössbauer time scale.[98] Numerous other examples of localization-to-delocalization transitions in mixed-valence biferrocenium salts and the influence of the crystallization solvent upon these transitions have also been discussed in detail.[99] Such complexity that originates from nonhomogeneity and weak interactions in solid phases of molecular complexes deserves further inquiry to aid in the development of materials that exhibit this phenomenological behavior.

Acknowledgment. K.R.D. acknowledges the National Science Foundation for a Nanoscale Science and Engineering (NIRT) Grant (DMR-0103455) and is grateful for equipment grants to purchase the CCD X-ray equipment (CHE-9807975) and the SQUID magnetometer (NSF-9974899). C.A. acknowledges Carnegie Mellon University for financial support. We thank Dr. Michael Hendrich for the use of his EPR instrumentation and EPR simulation software and Sebastian Stoian for technical assistance.

Supporting Information Available: Crystallographic files for **1**−**4** in CIF format, crystallographic data and structural refinement parameters for **1** over the 30−293 K temperature range before and after removal of weak reflection data using SQUEEZE, a full listing of bond distances and angles for **1**−**3**, supplementary Mössbauer spectra and ESI-MS data for **1**, and crystal packing diagrams and magnetic data for **3**. This material is available free of charge via the Internet at http://pubs.acs.org.

JA043162U

(98) Achim, C.; Bominaar, E. L.; Staples, R. J.; Munck, E.; Holm, R. H. *Inorg. Chem.* **2001**, *40*, 4389−4403.
(99) Hendrickson, D. N. *NATO ASI Series C* (Kluwer Academic Publishers: Dordrecht) **1991**, *343*, 67−90.